doi:10.1093/brain/awaa273 BRAIN 2020: 143; 3273–3293 | 3273

BRAIN
A JOURNAL OF NEUROLOGY

Splicing machinery dysregulation drives glioblastoma development/aggressiveness: oncogenic role of SRSF3

Antonio C. Fuentes-Fayos,[1,2,3,4,5] Mari C. Vázquez-Borrego,[1,2,3,4,5] Juan M. Jiménez-Vacas,[1,2,3,4,5] Leire Bejarano,[6] Sergio Pedraza-Arévalo,[1,2,3,4,5] Fernando L.-López,[1,2,3,4,5] Cristóbal Blanco-Acevedo,[1,3,7] Rafael Sánchez-Sánchez,[1,3,8] Oscar Reyes,[1,9] Sebastián Ventura,[1,9] Juan Solivera,[1,3,7] Joshua J. Breunig,[10,11,12,13,14] María A. Blasco,[6] Manuel D. Gahete,[1,2,3,4,5] Justo P. Castaño[1,2,3,4,5] and Raúl M. Luque[1,2,3,4,5]

Glioblastomas remain the deadliest brain tumour, with a dismal ~12–16-month survival from diagnosis. Therefore, identification of new diagnostic, prognostic and therapeutic tools to tackle glioblastomas is urgently needed. Emerging evidence indicates that the cellular machinery controlling the splicing process (spliceosome) is altered in tumours, leading to oncogenic splicing events associated with tumour progression and aggressiveness. Here, we identify for the first time a profound dysregulation in the expression of relevant spliceosome components and splicing factors (at mRNA and protein levels) in well characterized cohorts of human high-grade astrocytomas, mostly glioblastomas, compared to healthy brain control samples, being *SRSF3*, *RBM22*, *PTBP1* and *RBM3* able to perfectly discriminate between tumours and control samples, and between proneural-like or mesenchymal-like tumours versus control samples from different mouse models with gliomas. Results were confirmed in four additional and independent human cohorts. Silencing of *SRSF3*, *RBM22*, *PTBP1* and *RBM3* decreased aggressiveness parameters *in vitro* (e.g. proliferation, migration, tumorsphere-formation, etc.) and induced apoptosis, especially *SRSF3*. Remarkably, *SRSF3* was correlated with patient survival and relevant tumour markers, and its silencing *in vivo* drastically decreased tumour development and progression, likely through a molecular/cellular mechanism involving PDGFRB and associated oncogenic signalling pathways (PI3K-AKT/ERK), which may also involve the distinct alteration of alternative splicing events of specific transcription factors controlling PDGFRB (i.e. *TP73*). Altogether, our results demonstrate a drastic splicing machinery-associated molecular dysregulation in glioblastomas, which could potentially be considered as a source of novel diagnostic and prognostic biomarkers as well as therapeutic targets for glioblastomas. Remarkably, *SRSF3* is directly associated with glioblastoma development, progression, aggressiveness and patient survival and represents a novel potential therapeutic target to tackle this devastating pathology.

1 Maimonides Biomedical Research Institute of Cordoba (IMIBIC), 14004 Cordoba, Spain
2 Department of Cell Biology, Physiology and Immunology, University of Cordoba, 14004 Cordoba, Spain
3 Reina Sofia University Hospital (HURS), 14004 Cordoba, Spain
4 CIBER Physiopathology of Obesity and Nutrition (CIBERobn), 14004 Cordoba, Spain
5 Agrifood Campus of International Excellence (ceiA3), 14004 Cordoba, Spain
6 Telomeres and Telomerase Group, Molecular Oncology Program, Spanish National Cancer Research Centre (CNIO), 28029 Madrid, Spain
7 Department of Neurosurgery, Reina Sofia University Hospital, 14004 Cordoba, Spain
8 Pathology Service, Reina Sofia University Hospital, 14004 Cordoba, Spain
9 Department of Computer Sciences, University of Cordoba, 14004 Cordoba, Spain
10 Board of Governors Regenerative Medicine Institute, Cedars-Sinai Medical Center, Los Angeles, CA 90048, USA
11 Center for Neural Sciences in Medicine, Cedars-Sinai Medical Center, Los Angeles, CA 90048, USA

Received January 28, 2020. Revised June 17, 2020. Accepted July 5, 2020. Advance access publication November 3, 2020
© The Author(s) (2020). Published by Oxford University Press on behalf of the Guarantors of Brain.
This is an Open Access article distributed under the terms of the Creative Commons Attribution Non-Commercial License (http://creativecommons.org/licenses/by-nc/4.0/), which permits non-commercial re-use, distribution, and reproduction in any medium, provided the original work is properly cited. For commercial re-use, please contact journals.permissions@oup.com

12 Department of Biomedical Sciences, Cedars-Sinai Medical Center, Los Angeles, CA 90048, USA
13 Samuel Oschin Comprehensive Cancer Institute, Cedars-Sinai Medical Center, Los Angeles, CA 90048, USA
14 Department of Medicine, David Geffen School of Medicine, University of California, Los Angeles, CA 90095, USA

Correspondence to: Raúl M. Luque
IMIBIC Building. Av. Menéndez Pidal s/n. 14004-Córdoba, Spain
E-mail: raul.luque@uco.es

Keywords: glioblastoma; splicing machinery; SRSF3; PDGFRB pathway; antitumour therapy

Abbreviations: GBM = glioblastoma multiforme; HGA = high-grade astrocytoma

Introduction

Astrocytomas are a subtype of malignant gliomas characterized by rapid growth and high diffusion through the brain (Louis *et al.*, 2016). They are stratified from low to high aggressiveness (WHO criteria) (Louis *et al.*, 2016) with low-grade astrocytomas (grades I and II) and high-grade astrocytomas (HGAs; grades III and IV), and grade IV [glioblastoma multiforme (GBM)] being the most aggressive and one of the most common malignant cancers in the brain (14.7% of total) and the CNS (Ostrom *et al.*, 2018). Currently, HGAs/glioblastomas are detected by diagnostic imaging, with surgery as the first line of treatment, combined with chemotherapy and/or radiotherapy, depending on various clinical factors (type and degree of tumour, location and size, patient's age and sex, etc.). However, about two-thirds of patients with HGAs, mainly glioblastomas, do not have a survival rate >2 years after diagnosis (Ozdemir-Kaynak *et al.*, 2018).

Tumour pathologies, including HGAs, are known to share atypical presence, alteration or loss of relevant components of key molecular machineries regulating cell physiology, including the splicing machinery, which governs the splicing mechanism, that adequately processes the pre-mRNA to obtain mature mRNA (Chen and Manley, 2009; Pelechano *et al.*, 2013). Splicing is an intricate process, tightly regulated and carried out by the spliceosome (Yan *et al.*, 2019), a macromolecular machinery organized as a complex of RNA-protein multi-subunits, which act in a coordinated and sequential manner to develop its action in a highly dynamic way. Specifically, the spliceosome consists of a main core composed of five small nuclear ribonucleoproteins (SNRNPs), which is assisted by a large number of auxiliary core proteins and the so-called splicing factors (Jurica and Moore, 2003), which cooperate in the precise recognition of a multitude of target introns (Chen and Manley, 2009). In mammals there are two types of spliceosomes, the main or major spliceosome, also known as U2-dependent, and the minor, U12-dependent spliceosome (Chen and Manley, 2009; Matera and Wang, 2014).

Alternative splicing is not infrequent, as it is the mechanisms processing >90% of the human coding genes, and thereby provides an essential source of biological versatility. However, it is also a vulnerable regulatory point. Thus, growing evidence indicates that defects in the splicing process are frequent, leading to the appearance of altered spliceosome components, splicing factors and/or aberrant splicing variants (generated by alternative splicing), which are associated with the development, progression and aggressiveness of various types of cancer, such as lung, breast, prostate, colon, brain and pancreas (Stratton *et al.*, 2009; Cordoba-Chacon *et al.*, 2011; Guo *et al.*, 2015; Kozlovski *et al.*, 2017; Barbagallo *et al.*, 2018; Song *et al.*, 2019; Jimenez-Vacas *et al.*, 2020). In fact, the study of the expression profile of splicing isoforms ('splicing signature') has been shown in some tumours to provide a more useful tool than the analysis of the genetic/omic profile ('transcriptome signature') to provide an accurate classification of tumours/patients in terms of diagnosis and treatment selection (Feero *et al.*, 2010). Therefore, a better understanding of the regulation of splicing in normal and pathological tissues may help to identify novel diagnostic and prognostic biomarkers and therapeutic tools to target tumour pathologies.

However, to the best of our knowledge, no studies have reported hitherto a comprehensive analysis to ascertain whether the splicing machinery, i.e. the spliceosome and its auxiliary splicing factors, is altered in HGAs/glioblastomas. These data could provide new valuable avenues to develop novel strategies to tackle these terrible tumours. Thus, in this study we aimed to determine—for the first time—the expression profile of a representative set of spliceosome components and splicing factors and their relationship with key clinical and molecular features of glioblastoma samples/patients, as well as to determine the putative functional role and therapeutic potential of the most relevant components identified within this cellular machinery in this devastating disease.

Materials and methods

Reagents

Unless otherwise indicated, reagents and products were purchased from Sigma-Aldrich. Platelet-derived growth factor D (PDGFDD) (R&D systems, #1159-SB-025) was administered *in vitro* at 20 ng/ml based on a dose response experiment in glioblastoma cell lines (data not shown).

Patients and samples

Fresh HGAs/glioblastoma samples (AIII/IV; $n = 29$; Cohort-1) were obtained by intracranial surgery from patients previously diagnosed with HGAs/glioblastomas. Control brain tissue samples (CTs; $n = 16$) were obtained from four healthy donors [autopsy; four different brain areas (Brocca, Wernicke, cingulate and medial)] (Supplementary Table 1A). All samples were histologically studied by expert anatomopathologists to confirm as HGA/glioblastoma and control samples. Portions of each sample were rapidly frozen in liquid nitrogen and stored at −80°C until extraction for total RNA (see below) or formalin-fixed paraffin embedded (FFPE) for immunohistochemistry (IHC) analysis (see below). A validation cohort consisting of additional HGA/glioblastoma (AIII/IV; $n = 46$; Cohort-2) and control ($n = 3$; obtained by lobectomy surgery) samples were similarly obtained and analysed (Supplementary Table 1B). Demographic and clinical characteristics of both cohorts were collected to carry out clinical correlations. This study was approved by the Reina Sofia University Hospital Ethics Committee and was conducted in accordance with the principles of the Declaration of Helsinki. Written informed consent was obtained from all individuals included in the study.

Primary patient-derived glioblastoma cell culture

Glioblastoma samples were collected within 15 min after intracranial surgery and immediately transported to the cell culture room in sterile cold Spinner's modified Eagle medium (S-MEM) (Gibco, #11380-037) complemented with 0.1% bovine serum albumin (BSA) (#A2153), 0.01% L-glutamine (#G7513), 1% antibiotic-antimycotic solution (Gibco, #R01510) and 2.5% HEPES (#H3537). Glioblastoma samples were dispersed into single cells within the following 30 min by a mechanic/enzymatic protocol using 2% Collagenase IV (ThermoFisher-Scientific, #17104019) and 0.15% trypsin lyophilized powder (BD, #215310). Cell viability >90% was always obtained, as determined by the trypan-blue dye exclusion method. The single cells were cultured onto poly-L-lysine (#P1524-25MG) tissue culture plates in a 10% foetal bovine serum (FBS) (#F6765) containing Dulbecco's modified Eagle medium (DMEM) (BI, #06-1055-09-1A) complemented as S-MEM medium.

Cell lines

Glioblastoma cell lines (U-87 MG and U-118 MG) were obtained from the American Type Culture Collection (ATCC, #HTB-14/#HTB-15, respectively) and cultured according to the supplier's recommendations of passages <20. These cell lines were previously checked for mycoplasma contamination by PCR every month, as previously reported (Uphoff and Drexler, 2013).

PDGFA and PDGFB mouse models

All experimental procedures were carried out following the European Regulations for Animal Care, in accordance with guidelines and regulations, and under the approval of Ethics Committees (CEIyBA) from the Spanish National Cancer Research Centre (CNIO). Samples from two glioblastoma mouse models recently reported were used (PDGFA and PDGFB models; tumour and non-tumour samples) (Bejarano *et al.*, 2017).

Electroporated mouse models

All experimental procedures were performed according to the Cedars-Sinai Institutional Animal Care and Use Committee. Paired-end bulk RNAseq datasets from glioma mouse models generated by postnatal lateral ventricle electroporation after a plasmid DNA mix injection with driver mutations, which had been identified as driver mutations in previous models or in patient tumours (*Erbb2-V664E-EGFP/Hras-G12-EGFP/Kras-G12V-EGFP* tumour versus *EGFP* control models) were used as previously described (Breunig *et al.*, 2016).

RNA isolation, real-time qPCR and customized qPCR dynamic array based on microfluidic technology

Total RNA from fresh normal and tumour human and mouse tissue samples was extracted, followed by DNase treatment using the AllPrep DNA/RNA/Protein Mini Kit and the RNase-Free DNase set (Qiagen, #80004/#79254), respectively. Total RNA from glioblastoma cell lines was extracted with TRIzol® Reagent (ThermoFisher Scientific, #15596026). In all cases, total RNA concentration and purity were assessed by Nanodrop One Microvolume UV-Vis Spectrophotometer (ThermoFisher Scientific). For qPCR analyses, total RNA was retrotranscribed by using random hexamer primers and the RevertAid RT Reverse Transcription Kit (ThermoFisher Scientific, #K1691). Thermal profile and qPCR analysis to obtain absolute mRNA copy number/50 ng of sample of selected genes are reported elsewhere (Luque *et al.*, 2013, 2015).

As recently reported (Jimenez-Vacas *et al.*, 2019*b*, 2020), a qPCR dynamic array based on microfluidic technology (Fluidigm, #BMK-M-48.48) was implemented to determine the simultaneous expression of 48 transcripts in HGA/glioblastoma samples compared to control samples using the Biomark System and the Fluidigm® Real-Time PCR Analysis Software v.3.0.2 and Data Collection Software v.3.1.2 (Fluidigm). Specific primers for human and mouse transcripts including components of the major spliceosome ($n = 13$), minor spliceosome ($n = 4$), associated splicing factors ($n = 28$), PDGFRB pathway-related genes and three housekeeping genes were specifically designed with the Primer3 software (Supplementary Tables 2–4). To control for variations in the efficiency of the retrotranscription reaction, mRNA copy numbers of the different transcripts analysed were adjusted by a normalization factor, calculated with the expression levels of three housekeeping genes [β-actin (*ACTB*), hypoxanthine guanine phosphoribosyl-transferase (*HPRT*), glyceraldehyde 3-phosphate dehydrogenase (*GAPDH*; only for human samples) and peptidylprolyl isomerase-A (Cyclophilin A; only for mouse samples)] (Supplementary Tables 2 and 3) and the GeNorm v.3.3 software as previously reported (Luque *et al.*, 2015; Hormaechea-Agulla *et al.*, 2017*a*; Jimenez-Vacas *et al.*, 2019*a*).

Immunohistochemical analysis

IHC analysis of selected splicing factors was performed on FFPE samples obtained by intracranial surgery from patients diagnosed

with HGAs/glioblastomas (Cohort-1) and control/non-pathological samples. Specifically, rabbit polyclonal antibodies against human SRSF3 and RBM22 (#ab73891 and #ab59157, respectively), goat polyclonal antibody against human PTBP1 (#ab5642) and mouse monoclonal antibody against human RBM3 (#ab211356) were used following the manufacturer's instructions (Abcam). Specifically, deparaffinized sections were incubated with the antibody overnight at 4°C. Then, ImmPRESS® Anti-Mouse/Rabbit IgG Peroxidase (Vector Laboratories, #MP-7500-50) was used according to the supplier's recommendations, except for PTBP1 in which an anti-Goat IgG was added to secondary solution at a concentration of 1:500. Finally, sections were developed with 3,39-diaminobenzidine (Envision system 2-Kit Solution DAB, ThermoFisher Scientific, #34065), contrasted with haematoxylin (#MHS128). As previously reported (Del Rio-Moreno *et al.*, 2019; Jimenez-Vacas *et al.*, 2020), the pathologists performed histopathological analysis of the samples following a blinded protocol. In the analysis, +, ++, +++ indicate low, moderate, and high intensities of tumour region staining compared with the normal control adjacent region.

Silencing of splicing factors by specific small interfering RNA

Pre-designed and validated specific small interfering RNA (siRNA) oligos for knockdown of endogenous *SRSF3*, *RBM22* or *RBM3* (#s12733, #s31273, #s142991, respectively; Silencer® Select siRNAs; ThermoFisher Scientific), and for *PTBP1* (1:1 from B-C sequences; #SR303857; Trilencer-27 siRNA kit; Origene) were used. Cells ($n = 200\,000$ cells/well) were transfected with 25 nM of each siRNA individually using Lipofectamine RNAiMax® (ThermoFisher Scientific, #13778-075) according to the manufacturer's instructions. Silencer® Select Negative Control siRNA (ThermoFisher Scientific, #4390843) was used as a scramble control. After 48 h, cells were collected for validation of the transfection (qPCR and western blot) and seeded for different functional assays (see below).

Measurements of proliferation and migration rates

As previously described, cell proliferation (Hormaechea-Agulla *et al.*, 2017*b*; Vazquez-Borrego *et al.*, 2019) and migration (Hormaechea-Agulla *et al.*, 2017*a*, *b*; Vazquez-Borrego *et al.*, 2019) in response to *SRSF3/RBM22/PTBP1/RBM3* silencing or after PDGFDD treatment was analysed using alamarBlue® Assay (3000 cells/well for cell lines and 10 000 cells/well for primary cell cultures) (Biosource International, #BUF012B) and the wound-healing technique (150 000 U-118 MG cells/well), respectively. For the migration assay, U-118 MG cells cultured under confluence were serum-starved for 24 h to achieve cell synchronization, and, the wound was then made using a 200 µl sterile pipette tip. Wells were rinsed and cells were incubated for 6 h and 24 h with supplemented medium without FBS. Wound-healing was compared with the area just after the wound was performed. Three pictures were randomly acquired along the wound per well to calculate the area by ImageJ software v.1.49 (Schneider *et al.*, 2012).

Apoptosis analysis

As previously reported (Vazquez-Borrego *et al.*, 2019), apoptosis induction in response to *SRSF3/RBM22/PTBP1/RBM3* silencing in glioblastoma cell lines (5000 cells/well onto white-walled multi-well luminometer plates) was performed using Caspase-Glo® 3/7 Assay (Promega Corporation, #G8091). Cells were serum-starved for 24 h before the measurements, which were carried out following the manufacturer's protocols.

Tumorsphere formation

This assay was carried out in *SRSF3/RBM22/PTBP1/RBM3*-silenced glioblastoma cell lines (100 cells/well) cultured in a Corning Costar ultra-low attachment plate (#CLS3473) with DMEM F-12 (Gibco, #11320033) with EGF (20 ng/µl) (#SRP3027) for 10 days (refreshed every 48 h), as previously reported (Jimenez-Vacas *et al.*, 2019*a*). Briefly, an inverted microscope coupled to a digital camera was used to take photographs to visualize and measure cell morphology and area in order to calculate the number of tumorspheres after 10 days of incubation. Then, tumorspheres were trypsinized to determine the number of cells per tumorsphere. In addition, glioblastoma U-87 MG and U-118 MG cell lines were similarly analysed after 5 days of incubation with PDGFDD treatment (administered from time 0) combined with *SRSF3* silencing.

VEGF secretion

The VEGF Human ELISA Kit (ThermoFisher Scientific, #KHG0112) was used to quantify vascular endothelial growth factor (VEGF) secretion in response to *SRSF3/RBM22/PTBP1/RBM3* silencing in glioblastoma cell lines, following the manufacturer's instructions. Briefly, silenced cells were seeded (150 000 cells/well) and incubated for 24 h in FBS medium. Then, cells were starved in medium without FBS for 1 h and incubated under the same conditions for 4 h and 24 h. Medium was collected, centrifuged, and stored for VEGF determination.

Western blotting

To determine protein levels, cells pellets were resuspended using pre-warmed SDS-DTT sample buffer [62.5 mM Tris-HCl (#10708976001), 2% SDS (#71726), 20% glycerol (#17904), 100 mM DTT (#D0632-5G) and 0.005% bromophenol blue (#B0126)] followed by sonication for 10 s and boiling for 5 min at 95°C. Proteins were separated by SDS-PAGE and transferred to nitrocellulose membranes (Millipore, #1704270). Membranes were blocked with 5% non-fat dry milk (#T145.3), in Tris-buffered saline/0.05% Tween-20 (#93773) and incubated with the primary antibody [anti-SRSF3, anti-RBM22, anti-PTBP1, anti-RBM3, anti-AKT (CST, #4060S), anti-pAKT (CST, #9272S), anti-ERK1/2 (CST, #9102S), anti-pERK (CST, #4370S), anti-PDGFRB (CST, #3162) and anti-PIK3p110A (CST, #4249)], and their appropriate secondary antibodies [anti-rabbit IgG-HRP (CST, #7074), anti-mouse IgG-HRP (CST, #7076) or anti-goat IgG-HRP (#A9452)]. Proteins were developed using an enhanced chemiluminescence detection system (GE Healthcare) with dyed molecular weight markers. A densitometric analysis of the bands was carried out with ImageJ software v.1.49 (Schneider *et al.*, 2012) using total protein loading (Ponceau staining, #P3504-10G) or total protein signal (in case of AKT

and ERK) as normalizing factor, as previously reported (Jimenez-Vacas *et al.*, 2020).

Preclinical mouse model

A preclinical xenograft mouse model with silenced *SRSF3 in vivo* was developed. Specifically, 5-week-old ATHYM-*Foxn1*$^{nu/nu}$ mice ($n = 5$; Janvier Labs) were injected subcutaneously with 3×10^6 U-87 MG cells in both flanks [in 100 µl of basement membrane extract (Trevigen, #3432-010-01)]. Once the tumour was clearly measurable, each mouse received an injection with *SRSF3* siRNA into one flank and a negative control siRNA (used as a scramble control) into the other flank using AteloGene® reagent (KOKEN Co, #KKN1394) to transfect the siRNA molecule into cells by local administrations. Tumour growth was monitored every 4 days using a digital calliper. Sixteen days after injection, mice were sacrificed and each tumour was dissected, fixed, and sectioned for histopathological examination following haematoxylin and eosin staining. Examination of %KI67 and mitosis number was carried out by expert pathologists. Additional pieces from the tumour were in liquid nitrogen until RNA extraction using TRIzol reagent and protein extraction using SDS-DTT buffer, as previously reported (Jiménez-Vacas, 2019). These experiments were carried out according to the European Regulations for Animal Care under the approval of the university/regional government research ethics committees.

nCounter PanCancer signalling pathway analysis

As previously reported (Sarmento-Cabral *et al.*, 2017), the nCounter PanCancer Pathways Panel kit (NanoString Technologies, #GXA-PATH1-12) was used and carried out at the Laboratory of Genetics at UCAIB (IMIBIC) to simultaneously examine the expression of 730 genes associated with cancer (i.e. 606 genes representing all major cancer pathways and 124 key cancer driver genes). Briefly, after analysing the quality of all samples using microelectrophoresis, RNA from four scramble-control and four *SRSF3*-silenced samples from the preclinical mouse model (samples with the best quality) were loaded in the plate provided in the nCounter Kit, and the experiment was run following the manufacturer's protocol. The data were analysed using the nSolver Analysis Software v.4.0.66 from NanoString Technologies with the PanCancer Pathways Analysis Module using 36 genes as housekeeping genes. All specific target sequences and panel details are available on the manufacturer's webpage.

Detection of splicing variants in response to *SRSF3* silencing by end-point PCR

End-point PCR was developed using cDNA from glioblastoma cell lines in response to *SRSF3* silencing versus scramble-control to detect different splicing variants of *PDGFRB* and *TP73* (a *PDGFRB* transcription factor). Details of the end-point PCR to detect splicing events have previously been reported (Duran-Prado *et al.*, 2009; Hormaechea-Agulla *et al.*, 2016). Primer sequences are included in Supplementary Table 4.

Bioinformatics and statistical analysis

Several data-mining processes were carried out by bioinformatic experts (Supplementary Fig. 3A), ranging from the application of preprocessing methods to the construction of classification and clustering models for a better estimation of the relevance of specific factors. Data were evaluated for heterogeneity of variance using the Kolmogorov–Smirnov test. Statistical differences were assessed by *t*-test, Mann-Whitney U-test or by one-way ANOVA followed by Fisher's correction exact test. Analysis of qPCR array results was carried out by a bioinformatic expert who used several tests, models and hierarchical cluster algorithms, which allowed us to make a fairly accurate assessment. Correlations were studied using the Pearson correlation test. All statistical analyses were performed using Prism software v.8.0 (GraphPad Software, La Jolla, CA, USA) except the clustering analyses which were performed with MetaboAnalyst Software v.4.0 (McGill University, Quebec, Canada). Paired-end bulk RNAseq data were aligned, analysed and normalized using Partek Flow® software (Partek Incorporated, St. Louis, MO, USA). For survival analysis, groups were selected based on the cut-off points determined by survminer R package or median. The computational methodology shown in Supplementary Fig. 3A was implemented in R language v.3.5. Values of $P < 0.05$ were considered statistically significant. Data represent median (interquartile range) or means ± standard error of mean (SEM). $^*P$, 0.05; $^{**}P$, 0.01; $^{***}P$, 0.001, significantly different from control conditions.

Data availability

Microfluidic array, RNAseq, nCounter and other data used in this paper are available upon request to the corresponding author. Chinese Glioma Genome Atlas RNAseq data (CGGA) and Murat microarray data were interrogated through the GlioVis Tools (http://gliovis.bioinfo.cnio.es) (Murat *et al.*, 2008; Bowman *et al.*, 2017).

Results

Splicing machinery is drastically dysregulated in high-grade astrocytomas/glioblastomas

The expression levels of the components of the splicing machinery (spliceosome components and splicing factors) were analysed in HGAs/glioblastomas and control samples from a first cohort of patients (Supplementary Table 1A). An initial analysis in the four different brain areas obtained from healthy donors (control samples) revealed that the expression levels of all the splicing machinery components were completely homogenous across the different control brain areas (based on principal component analysis, PCA) (Supplementary Fig. 1A). Moreover, the individual expression level of these splicing machinery components did not vary across the four brain areas (based on qPCR analysis; data not shown). Similarly, PCA and individual mRNA

expression comparisons also revealed that expression levels of these splicing machinery components were completely homogeneous between grade III versus IV HGAs (n = 8 and 21, respectively) (Supplementary Fig. 1B and C). Based on these results, further analyses were performed combining the expression levels of the four different control brain areas of each patient (control tissues, CTs; n = 4), and both HGA samples (III and IV-glioblastoma, HGAs/glioblastomas; n = 29).

Remarkably, we found a marked dysregulation in the expression levels of multiple components of the splicing machinery (spliceosome components and splicing factors) in HGAs/glioblastomas compared to the control tissues. Specifically, there was a significant upregulation of the 11 major spliceosome components (*RBM22*, *PRPF8*, *PRPF40A*, *TCERG1*, *SF3B1*, *SF3B1TV1*, *U2AF2*, *U2AF1*, *RNU5*, *RNU4* and *RNU1*) and 20 splicing factors (*SNW1*, *TIA1*, *TRA2A*, *TRA2B*, *SRSF10*, *SRSF9*, *SRSF6*, *SRSF5*, *SRSF3*, *SRSF2*, *SRRM1*, *SND1*, *KHDRBS1*, *RBM45*, *RBM3*, *RAVER1*, *PTBP1*, *NOVA1*, *MAGOH* and *CELF1*), whereas two minor spliceosome components (*RNU11* and *RNU12*) and two splicing factors (*ESRP1* and *SRRM4*) were significantly downregulated (Fig. 1A and Supplementary Fig. 2). Interestingly, non-supervised hierarchical analysis based on the expression pattern of all spliceosome components and splicing factors was able to perfectly discriminate HGAs/glioblastomas and control tissues into two independent clusters (Fig. 1B), which was also confirmed by PCA (Fig. 1C). In fact, application of different bioinformatics analyses [i.e. five feature weighting and heuristic methods (Supplementary Fig. 3A), and variable importance in projection (VIP) score of partial least squares-discriminant analysis (PLS-DA; Fig. 1D)] revealed that *SRSF3*, *RBM22*, *PTBP1* and *RBM3* were always the highest score components, capable of discriminating between HGAs/glioblastomas and control tissues. Indeed, expression of these four components of the splicing machinery was elevated in HGAs/glioblastomas (Fig. 1E), and receiver operating characteristic (ROC) curve analyses corroborated their capacity to finely discriminate between HGAs/glioblastomas and controls samples, showing an area under the curve (AUC) of 1 (Fig. 1E). Moreover, as depicted in Fig. 1F, the heat map generated with only these four components perfectly discriminated HGAs/glioblastomas from control tissues, segregating them into two perfect clusters. Of note, overexpression of *SRSF3*, *RBM22*, *PTBP1* and *RBM3* levels in HGA/glioblastoma samples was further corroborated in a second cohort of patients collected in our hospital (validation cohort: three control tissues versus 46 HGAs/glioblastomas) (Supplementary Fig. 3B and Supplementary Table 1B), as well as in the well-characterized Murat and CGGA external dataset cohort available on the GlioVis data portal (Murat *et al.*, 2008; Bowman *et al.*, 2017). Furthermore, available data from the CGGA revealed that *SRSF3*, *PTBP1* and *RBM3*, but not *RBM22*, mRNA levels were increased across glioma grades (III versus IV; n = 288; Supplementary Fig. 3D and E). Moreover, and similar to that previously found in the first cohort (Fig. 1A–F), the expression levels of *SRSF3*, *RBM22*, *PTBP1* and *RBM3* in this validation cohort again allowed the perfect discrimination between HGAs/glioblastomas and control tissues into two perfect clusters (Supplementary Fig. 3C). Based on these results, we selected *SRSF3*, *RBM22*, *PTBP1* and *RBM3* for further analyses.

Protein levels of SRSF3, RBM22, PTBP1 and RBM3 are elevated in HGA/glioblastoma samples

Consistent with the results of mRNA, IHC analyses using FFPE of all the samples from the first cohort of patients (Supplementary Table 1A) revealed that nuclear protein levels of SRSF3, PTBP1 and RBM3 were significantly elevated in HGA/glioblastoma samples compared to control samples; however, RBM22 staining was not elevated in these HGA/glioblastoma samples (Fig. 1G). Interestingly, we also had the possibility to compare the levels of these four splicing machinery components in a glioblastoma tumour tissue versus its non-tumour adjacent tissue, which confirmed that the protein levels of all of these factors, including RBM22, were clearly elevated in the glioblastoma tissue compared to the non-tumour area (Supplementary Fig. 4). In addition, low levels of cytoplasmic staining of SRSF3 were detected in HGA/glioblastoma tissues, although the score did not reach statistical significance (data not shown). Furthermore, SRSF3, RBM22, PTBP1 and RBM3 protein overexpression was corroborated in GBMs versus non-tumour samples (GTEx tissues) using the proteomic glioblastoma CPTAC dataset (Edwards *et al.*, 2015) (Fig. 1H).

Dysregulation in splicing machinery is confirmed in different mouse models

We also studied the expression levels of the 45 splicing machinery components (the same as previously analysed in human HGAs/glioblastomas) in two mouse models with proneural-like glioblastoma (PDGFA model) and mesenchymal-like glioblastoma (PDGFB model) recently published (Ozawa *et al.*, 2014) (Fig. 2A), as well as in electroporated glioma mouse models with constitutively active oncogenes (*Erbb2-V664E-EGFP/Hras-G12-EGFP/Kras-G12V-EGFP* tumour versus *EGFP*-control model) as previously described (Breunig *et al.*, 2016) (Fig. 3A).

Similar to that observed in humans, a marked dysregulation of the splicing machinery components was found in the PDGF mice and electroporated mice tumour samples (Figs 2B and 3B, respectively). Specifically, non-supervised hierarchical analysis based on the expression pattern of all these components was able to perfectly separate tumour and control samples into two independent clusters (Figs 2B and 3B). Fifteen of these components were commonly dysregulated in human and both mouse PDGF models (Fig. 2C), including the four key components (*Srsf3*, *Rbm22*, *Ptbp1*

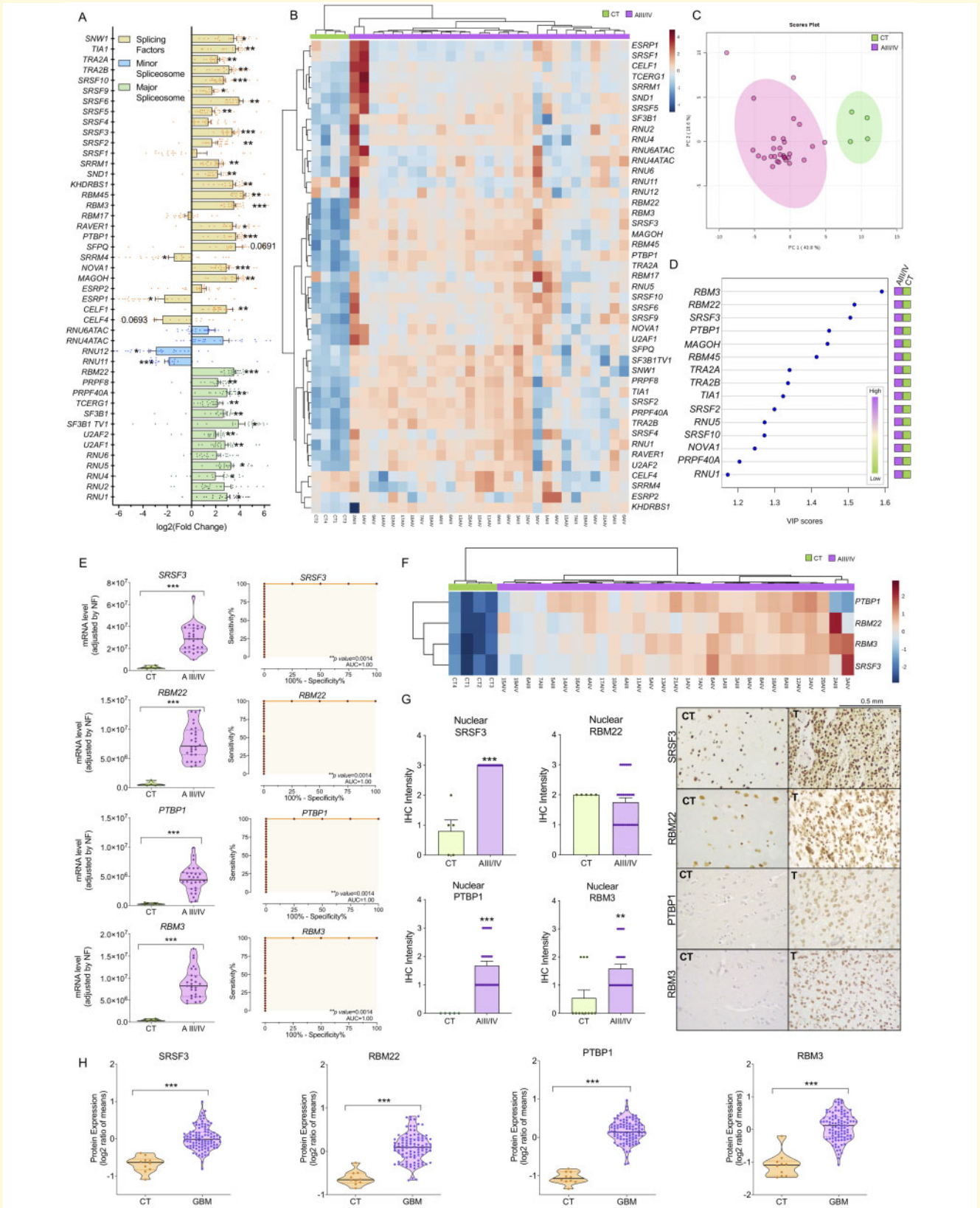

Figure 1 Splicing machinery is drastically dysregulated in HGAs/glioblastomas. (**A**) Individual fold-change of the expression of all the splicing machinery components analysed in control brain tissues (CT) and HGA/glioblastoma samples. (**B**) Hierarchical heat map generated using the expression levels of all the spliceosome components and splicing factors determined in control brain tissues from different brain areas [Controls (Brocca, Wernicke, cingulate and medial); $n = 4$] and HGA/glioblastoma samples (grades AIII/AIV; $n = 29$). (**C**) Principal components analysis of the mRNA expression levels of the splicing machinery components in the same sample set. (**D**) VIP scores obtained from partial least

(continued)

and *Rbm3*) previously selected in human samples. Likewise, 22 components were also commonly dysregulated in human and the electroporated mouse models, including *Srsf3*, *Ptbp1* and *Rbm3*, but not *Rbm22* (Fig. 3C). In fact, ROC curve analyses of these four components corroborated their capacity to significantly discriminate between tumour and control tissues showing an AUC for *Srsf3*, *Rbm22*, *Ptbp1* and *Rbm3* of 1, 0.78, 1 and 0.89 in the PDGFA model, of 1, 1, 1 and 0.81 in the PDGFB-model, and of 1, 0.5, 1 and 1 in the electroporated glioma models, respectively (Figs 2D and 3D). Moreover, heat maps and PCA generated with these four components in PDGF and electroporated mouse models clearly showed that the expression pattern of just these four components is able to separate tumour and control tissues, segregating them into two perfect clusters/groups (Figs 2E and 3E).

In addition, western blot analyses using the PDGF samples revealed that protein levels of Srsf3, Rbm22, Ptbp1 and Rbm3 were significantly elevated in glioblastoma samples compared to their control tissues in both mouse models (Srsf33 expression tended to be elevated in the PDGFB model; $P = 0.125$; Fig. 2F). Moreover, analysis of the RNAseq dataset from the electroporated glioma models revealed that only *Srsf3* expression was significantly higher in mesenchymal-like models in comparison with proneural-like models (Fig. 3F).

Silencing of *SRSF3*/*RBM22*/*PTBP1*/*RBM3* expression decreases functional parameters in glioblastoma cells

Two human glioblastoma cell line models (U-87 MG and U-118 MG) and/or primary patient-derived glioblastoma cell cultures were used to perform functional experiments (Fig. 4A). First, a heat map and a PCA generated with the expression pattern of all spliceosome components and splicing factors (Supplementary Fig. 5A and B) and also with only *SRSF3*, *RBM22*, *PTBP1* and *RBM3* (Supplementary Fig. 5A) were able to perfectly separate human control tissues into independent clusters/groups from human HGA/glioblastoma tissues and glioblastoma cell lines. In addition, data from available GBM cell lines ($n = 34$, including U-87 MG and U-118 MG) and primary GBM lines ($n = 12$) RNAseq were also analysed (Cancer Cell Line Encyclopedia) (Ghandi *et al.*, 2019; Stringer *et al.*, 2019), which revealed a similar expression profile of the spliceosome components and splicing factors across the different models, indicating that the U-87 MG and U-118 MG cell models used herein were appropriate glioblastoma models to study the functional role of the selected splicing machinery components (Supplementary Fig. 5C–E).

Silencing of *SRSF3*, *RBM22*, *PTBP1* and *RBM3* (confirmed at the mRNA and/or protein levels; Supplementary Fig. 5F) significantly decreased proliferation rate in a time-dependent manner in both glioblastoma cell lines and in primary patient-derived glioblastoma cell cultures (Fig. 4B). Similarly, silencing of these components reduced migration rate in a time-dependent manner in U-118 MG (Fig. 4C). Specifically, *SRSF3*, *RBM22* and *RBM3* silencing decreased migration capacity at 6 h and 24 h, but this difference did not reach statistical significance in the case of RBM22 (Fig. 4C). *PTBP1* silencing significantly decreased migration only at 6 h (Fig. 4C). Moreover, a clear decrease in VEGF secretion was observed after *SRSF3* and *PTBP1* silencing in both cell lines, while RBM3 silencing decreased VEGF secretion only in U-87 MG cells, and a trend for statistical significance was found in response to *RBM22* silencing in both cell lines (Fig. 4D). Furthermore, the use of the capase3/7 assay revealed that *SRSF3* silencing induced apoptosis in both glioblastoma cells models, while *RBM3* silencing only increased apoptotic rate in U-118 MG cells (Fig. 4E). Finally, application of a tumorsphere formation assay to quantify the proliferation capacity of cancer stem/progenitor cells revealed that *SRSF3*, *RBM22*, *PTBP1* and *RBM3* silencing decreased the number of glioblastoma stem/progenitor cells present in each tumorsphere in both cell lines (Fig. 4F).

Dysregulation of the splicing machinery is associated with relevant clinical parameters

Low expression of *SRSF3* (Fig. 5A), but not *RBM22*, *PTBP1* and *RBM3* (Supplementary Fig. 6A), was directly associated with better survival rate in glioblastoma patients from the first cohort. It should be noted that this analysis could not be implemented in our second cohort (validation cohort) as these patients were diagnosed near the end of the study. Nonetheless, we could also corroborate that *SRSF3*

Figure 1 Continued
squares discriminant analysis (PLS-DA) of all of the splicing machinery components studies. (**E**) Levels of mRNA from selected splicing machinery components (*SRSF3*, *RBM22*, *PTBP1* and *RBM3*) in control and tumour tissues and ROC curves analysis. (**F**) Hierarchical heat map generated using the expression levels of selected splicing machinery components (*SRSF3*, *RBM22*, *PTBP1* and *RBM3*) in control brain tissues from different brain areas (CTs) and HGAs/glioblastomas (grades AIII/AIV). (**G**) IHC analysis of nuclear levels of SRSF3, RBM22, PTBP1 and RBM3 in FFPE samples from control and HGA/glioblastoma tissues (representative images are depicted). (**H**) Protein expression levels of SRSF3, RBM22, PTBP1 and RBM3 in GBM compared to non-tumour samples (GTEx tissues) using the proteomic glioblastoma CPTAC dataset. Data represent median (interquartile range) or means ± SEM. **P*, 0.05; ***P*, 0.01; ****P*, 0.001, significantly different from control conditions. See also Supplementary Figs 1–4.

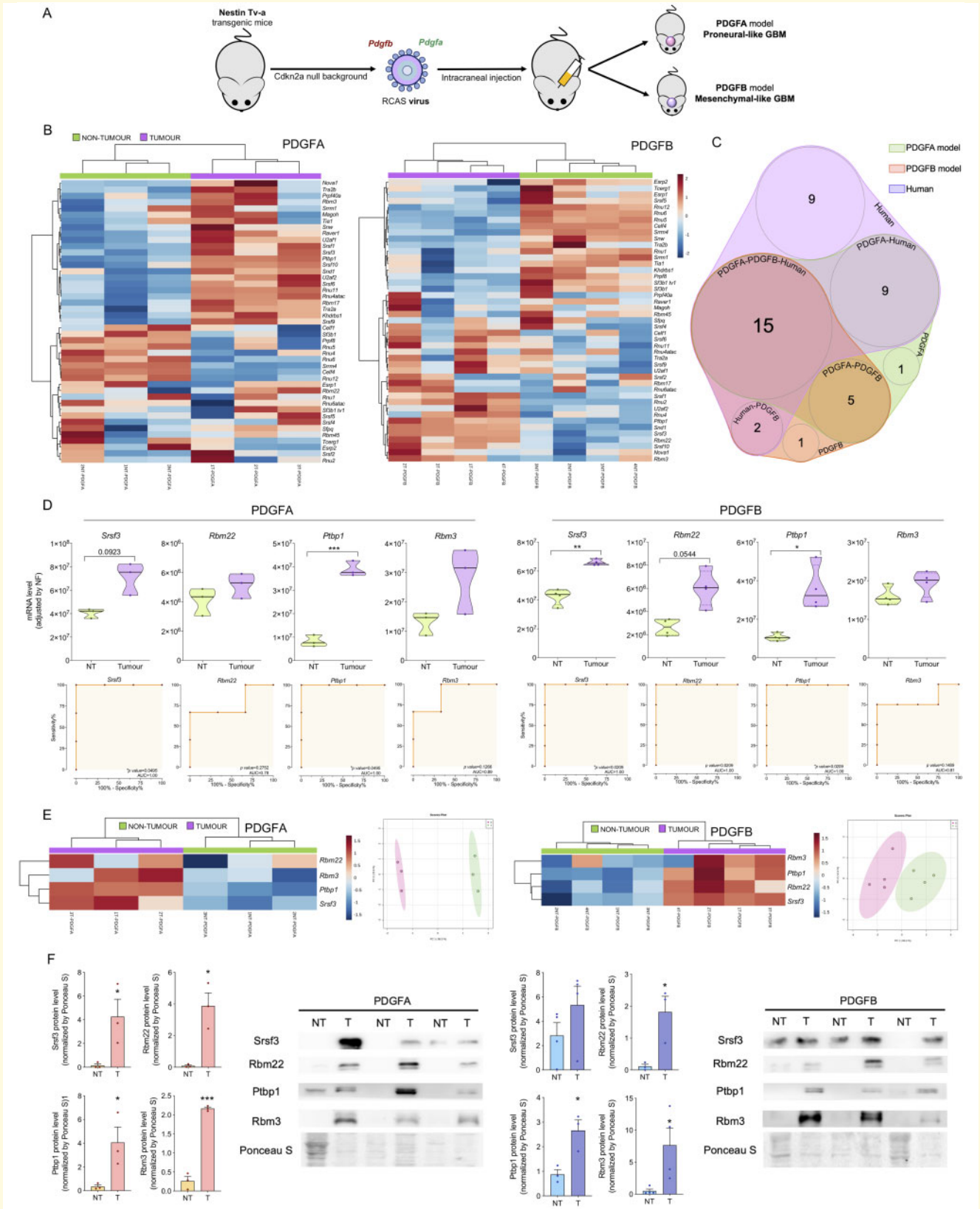

Figure 2 Dysregulation in the splicing machinery is also confirmed in two mouse models with proneural-like and mesenchymal-like glioblastoma. (**A**) Diagram of generation of mouse models of glioblastoma by overexpression of PDGFB or PDGFA in a Cdkn2a null background in Nestin-expressing cells (adapted from Bejarano *et al.*, 2017). (**B**) Hierarchical heat map generated using the mRNA expression levels of spliceosome components and splicing factors in non-tumour and tumour samples from PDGFA/B-induced mouse models. (**C**) Venn diagram of altered splicing machinery components in PDGFA/B-induced glioblastoma mouse models and human HGA/glioblastoma samples.

(continued)

expression was directly associated with a better survival rate in glioblastoma patients using the well-characterized Murat and CGGA dataset (Fig. 5B and C), this association being with *SRSF3*, but not with *RBM22*, *PTBP1* and *RBM3*, consistent across the different datasets (Supplementary Fig. 6B and C). In line with this association, a higher expression of *SRSF3* (Supplementary Fig. 6E; CGGA dataset), but not *RBM22*, *PTBP1* and *RBM3* (data not shown), was found in human mesenchymal GBM subtype (a poor survival GBM subtype) compared to proneural GBM subtype. Consistently, we found that the difference in mouse *Srsf3* expression levels was more evident, in terms of *P*-values, when comparing mesenchymal GBM subtype versus control samples than in the case of proneural GBM subtype versus control samples in both mouse models analysed (PDGF and electroporated mice; Supplementary Fig. 6F). Additionally, we found a significant correlation between *SRSF3* (Fig. 5D), but not *RBM22, PTBP1* and *RBM3* (Supplementary Fig. 6D), with the %KI67 index, a standard proliferative marker, in our cohort of patients. Likewise, a correlation between expression levels of *SRSF3* and those of different key tumour progression markers (*MKI67*, *PCNA*, *CDK1* and *CCNB1*) was also found in glioblastoma tissues (Murat and CGGA dataset), but not in the non-tumour samples (available only in Murat dataset) (Fig. 5E and F). Based on these and the previous results, *SRSF3* was selected to perform further studies.

SRSF3 silencing prevents the progression of glioblastomas *in vivo*

SRSF3 silencing *in vivo* (validated at mRNA and protein levels; Supplementary Fig. 7A and B) reduced tumour volume and weight in the preclinical xenograft glioblastoma model (Fig. 6A). In fact, *in vivo* tumour volume across time clearly showed that glioblastoma progression was completely stopped in the *SRSF3*-silenced model (blue line) compared to the scramble-transfected tumours, which drastically continued their progression (green line; Fig. 6A). Moreover, the number of mitosis and %KI67 IHC staining was significantly decreased in the *SRSF3*-silenced model compared to the scramble-transfected (Fig. 6B) supporting the strong anti-tumour potential of *SRSF3* silencing in glioblastoma cells previously observed *in vitro* (Fig. 4) and *in vivo* (Fig. 6A).

SRSF3 silencing alters multiple key cancer-related pathways *in vivo*

SRSF3 silencing *in vivo* significantly altered the expression of 149 of 770 genes analysed with the nCounter PanCancer Pathways Panel kit compared to the scramble-transfected tumours (Fig. 6C). Specifically, the PI3K pathway was the most altered signalling pathway (i.e. 39 genes: 23 downregulated/16 upregulated), followed by the cell cycle and apoptosis pathways (i.e. 35 genes: 25 upregulated/10 downregulated; Fig. 6D). Additionally, other key signalling pathways were also altered (e.g. RAS, MAPK, Wnt, DNA-damage/repair, transcription misregulation, etc.) (Fig. 6D). Indeed, the heat maps generated with the genes involved in several of these pathways were able to perfectly discriminate between *SRSF3*-silenced versus scramble-transfected glioblastoma cells (Supplementary Fig. 8A).

We next used the STRING database to determine the potential functional association between the altered genes in response to *SRSF3*-silencing (Fig. 6E), which showed the existence of three clusters of altered genes strongly associated with the control of cell cycle/transcription/DNA replication (cluster-1: blue), PDGFR-activated pathway (cluster-2: magenta) and focal adhesion (cluster-3: green). An additional protein–protein interaction (PPI) functional association performance by Network Analyst software, revealed that the PDGFRB-activated pathway was the most relevant pathway altered (Supplementary Fig. 8B). In fact, a specific analysis of the glioma pathway using KEGG revealed a clear alteration in several genes involved in the PDGFRB pathway (i.e. *PDGFRB*, *SOS2*, *SHC2*, *PIK3CR3* and *PIK3CA*) (Fig. 6E), which further supported the relevance of the *PDGFRB* in *SRSF3*-silenced cells.

PDGFRB pathway inhibition as a driver of *SRSF3* silencing-induced anti-glioblastoma tumour actions

mRNA levels of the glioma pathway components *PDGFRB*, *SOS2*, *SHC2*, *PIK3CR3* and *PIK3CA* were significantly downregulated in *SRSF3*-silenced xenografted glioblastoma cells (Fig. 7A). Similarly, these changes were also observed in U-87 MG, U-118 MG and patient-derived primary glioblastoma cell cultures (Supplementary Fig. 9A). A protein downregulation of upstream (i.e. PDGFRB and PIK3 catalytic α-subunit) components of the glioma-pathway was also found in *SRSF3*-silenced xenografted glioblastoma cells (Fig. 7A), and also observed (i.e. PDGFRB) in U-87 MG and

Figure 2 Continued
(**D**) Expression levels of mRNA and ROC curve analysis of selected splicing machinery components in PDGFA/B-induced mouse model samples. (**E**) Hierarchical heat map generated using the mRNA expression levels of previously selected splicing machinery components in the human study (*Srsf3*, *Rbm22*, *Ptbp1* and *Rbm3*) and the PCA in the same set of murine samples. (**F**) Analysis and western blot images showing the validation of SRSF3, RBM22, PTBP1 and RBM3 protein overexpression in PDGFA/B-induced mouse tumours. Data represent median (interquartile range) or means ± SEM. **P*, 0.05; ***P*, 0.01; ****P*, 0.001, significantly different from control conditions.

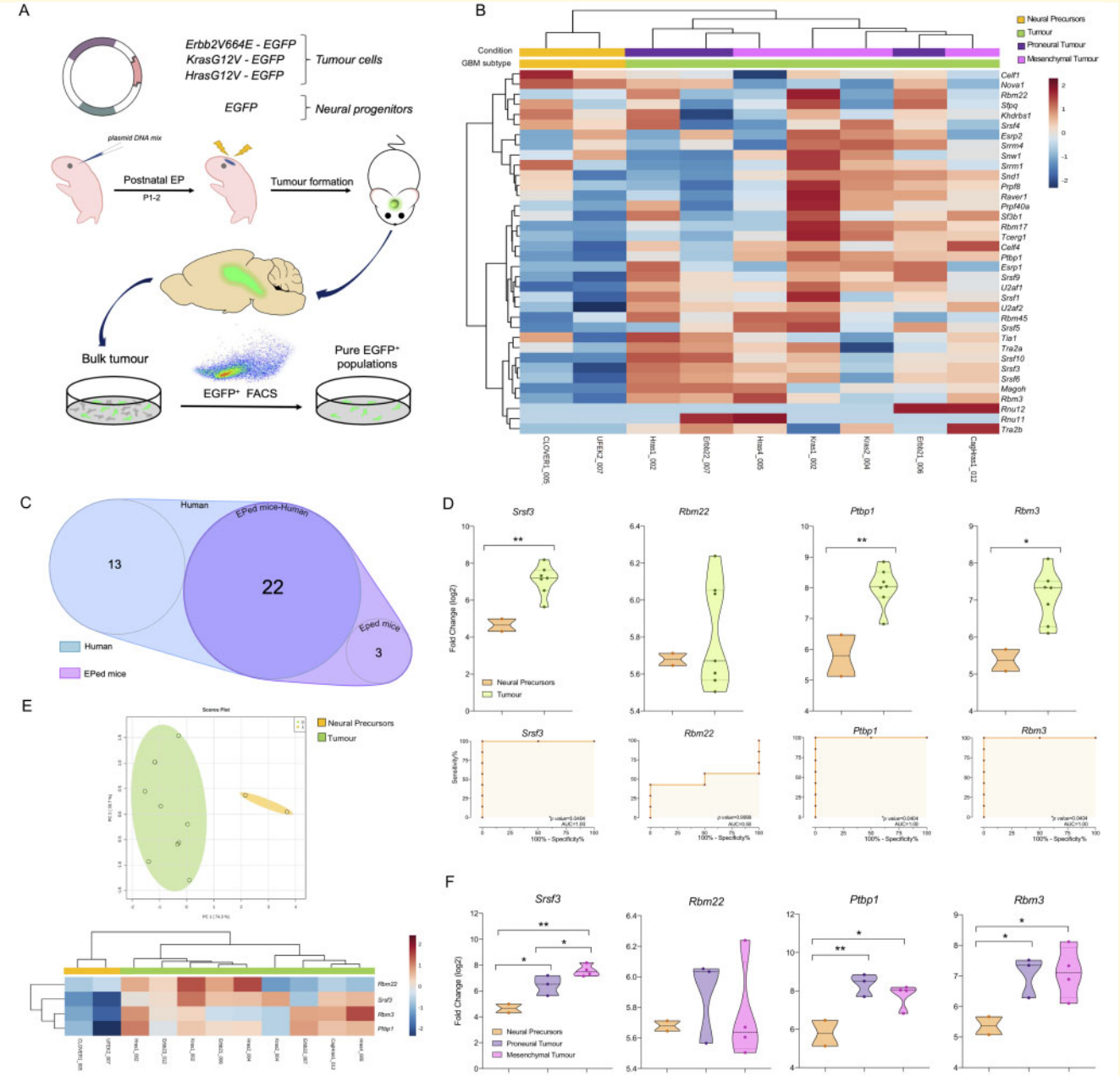

Figure 3 Dysregulation in the splicing machinery is also confirmed in electroporated glioma mouse models. (**A**) Diagram of the generation of mouse models of glioblastoma by plasmid DNA mix injection into the left lateral ventricle following mouse brain electroporation (EP) (adapted from Breunig *et al.*, 2016). (**B**) Hierarchical heat map generated using the mRNA expression levels of spliceosome components and splicing factors in non-tumour and tumour samples classified in mesenchymal-like and proneural-like from electroporated models. (**C**) Venn diagram of altered splicing machinery components in electroporated (EPed) models and human HGA/glioblastoma samples. (**D**) mRNA expression levels and ROC curve analysis of selected splicing machinery components in the electroporated mouse model samples. (**E**) Hierarchical heat map generated using the mRNA expression levels of previously selected splicing machinery components in the human study (*Srsf3*, *Rbm22*, *Ptbp1* and *Rbm3*) and the PCA in the same set of murine samples. (**F**) mRNA expression levels of selected splicing machinery components in the electroporated mouse model samples classified in proneural-like or mesenchymal-like phenotype versus control samples (neural precursors). Data represent median (interquartile range) or means ± SEM. **P*, 0.05; ***P*, 0.01; ****P*, 0.001, significantly different from control conditions.

U-118 MG cells (Fig. 7B and Supplementary Fig. 9B). In addition, inhibition of total protein levels of the downstream components of the PDGF-PDGFRB pathway [i.e. AKT and ERK (classical end points of this pathway associated with cell survival, cell growth and cell proliferation)] was also observed in *SRSF3*-silenced xenografted glioblastoma cells (Fig. 7A) and/or *SRSF3*-silenced glioblastoma cells *in vitro* (U-87 MG and U-118 MG; Fig. 7B). Interestingly, we found

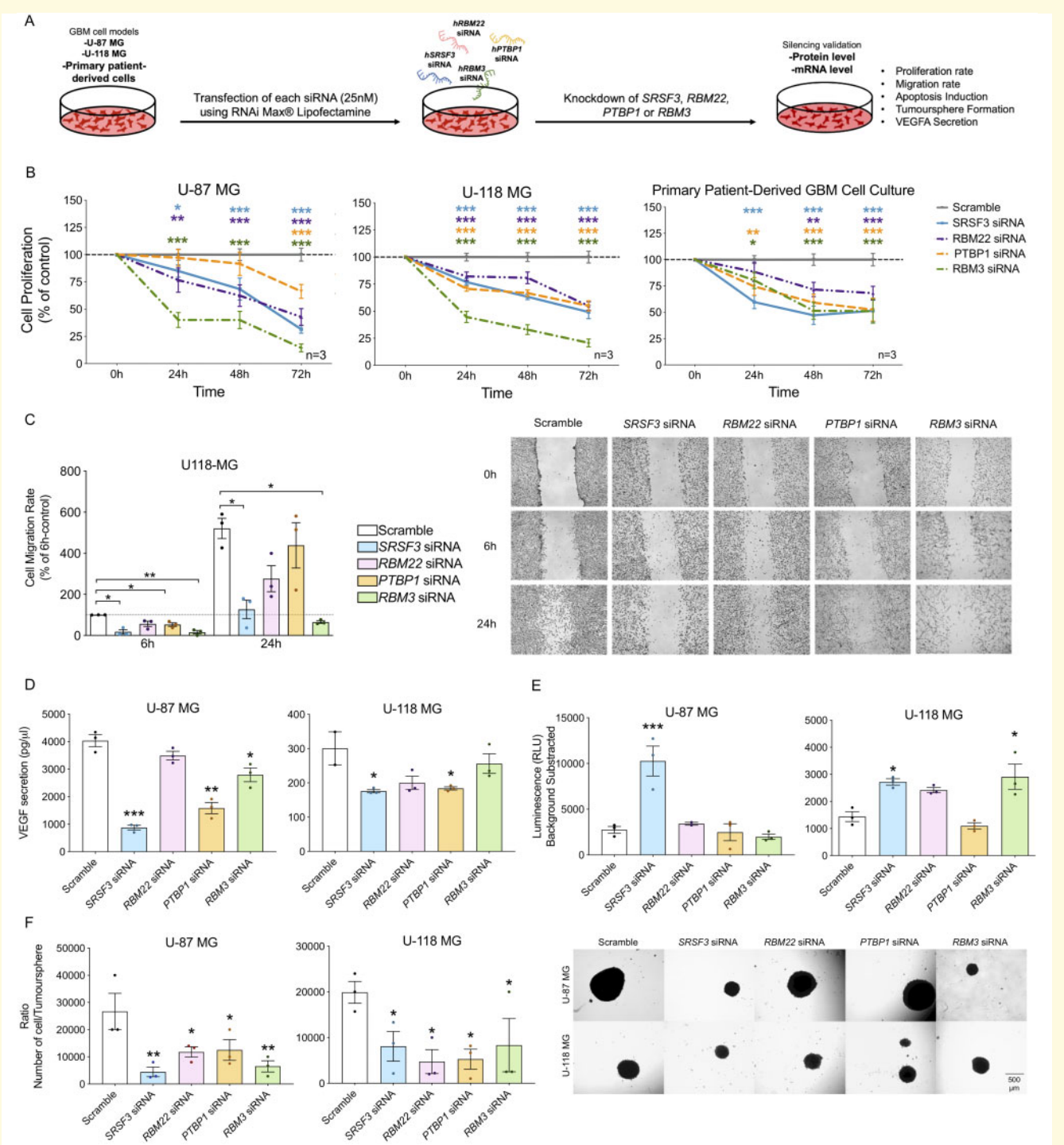

Figure 4 Silencing of *SRSF3, RBM22, PTBP1* and *RBM3* expression decreases functional parameters of aggressiveness in glioblastoma cell lines and primary patient-derived glioblastoma cells. (**A**) Diagram showing the *in vitro* generation of *SRSF3*, *RBM22*, *PTBP1* and *RBM3* knockdown glioblastoma cells by silencing with specific siRNAs. (**B**) Proliferation rate of *SRSF3*, *RBM22*, *PTBP1* and *RBM3*-silenced cells compared to control scramble-transfected cells (U-87 MG and U-118 MG models and primary patient-derived glioblastoma cells; $n = 3$). (**C**) Migration rate of *SRSF3*, *RBM22*, *PTBP1* and *RBM3*-silenced U-118 MG cells compared to control scramble-transfected cells (representative images of the migration capacity are also included; $n = 3$). (**D**) VEGF secretion of *SRSF3*, *RBM22*, *PTBP1* and *RBM3*-silenced cells compared to control scramble-transfected cells (U-87 MG and U-118 MG models; $n = 3$). (**E**) Apoptosis levels in *SRSF3, RBM22, PTBP1* and *RBM3*-silenced cells compared to control scramble-transfected cells (U-87 MG and U-118 MG models; $n = 3$). (**F**) Number of cells per tumorsphere and representative images of formation of tumorspheres in *SRSF3*, *RBM22*, *PTBP1* and *RBM3*-silenced cells compared to control scramble-transfected cells on cell morphology (U-87 MG and U-118 MG models; $n = 3$). Data represent means ± SEM. **P*, 0.05; ***P*, 0.01; ****P*, 0.001, significantly different from control conditions. See also Supplementary Fig. 5.

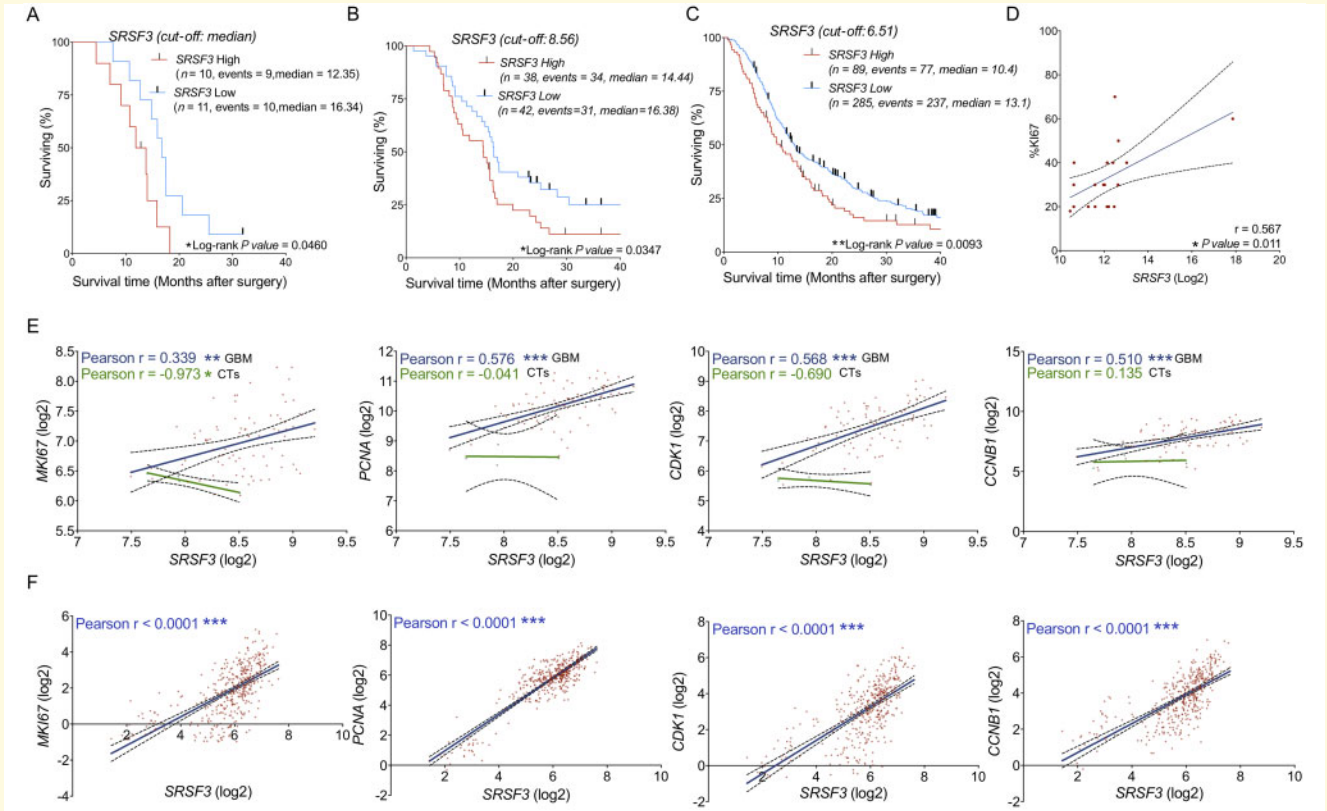

Figure 5 The dysregulation of the splicing machinery is associated with relevant clinical parameters. Kaplan-Meier survival curves discerning between glioblastoma patients with high and low expression levels of *SRSF3* from our cohort of patients (**A**), from the Murat dataset (**B**), and from the CGGA dataset (**C**). Correlation of *SRSF3* mRNA expression levels and %KI67 in glioblastoma patients (**D**). Correlation of *SRSF3* with different prognostic biomarkers in glioblastoma samples (blue regression line) and CTs (green regression line) using the Murat dataset (**E**). Correlation of *SRSF3* with different prognostic biomarkers in glioblastoma samples using the CGGA dataset (**F**). See also Supplementary Fig. 6.

that only the phosphorylation levels of ERK, but not AKT, were significantly downregulated in *SRSF3*-silenced glioblastoma cells *in vitro* (U-87 MG and U-118 MG; Fig. 7B). Remarkably, silencing of *SRSF3* completely blocked the pro-oncogenic parameters (i.e. proliferation and number of glioblastoma stem/progenitor cells) induced in response to PDGFDD (specific ligand of PDGFRB receptor) in glioblastoma cells *in vitro* (U-87 MG and U-118 MG; Fig. 7C and D). Similar results in terms of proliferation rate were also observed in patient-derived glioblastoma primary cell cultures (Fig. 7C). Supporting these results is the fact that *SRSF3*-silencing blocked the stimulatory effects on AKT and ERK pathways induced by PDGFDD treatment in glioblastoma cells (U-87 MG and U-118 MG) (Fig. 7E).

Changes in the expression of *TP73* splicing variants as functional link between SRSF3-PDGF-PDGFRB pathway

Our results indicate that *SRSF3* silencing does not alter the splicing of *PDGFRB* in GBM cell lines (Supplementary Fig. 10A) thus arguing against a direct action of this splicing factor on the receptor itself. Of note, our present results on *SRSF3* silencing compare favourably with those in the Song *et al.* (2019) dataset, where *SRSF3* knockout also downregulated *PDGFRB* (Supplementary Fig. 10B), while not altering *PDGFRB* splicing. Thus, to explore alternative mechanisms possibly linking SRSF3 and PDGF-PDGFRB pathway, we interrogated various datasets, aiming to ascertain the potential involvement of *PDGFRB*-controlling transcription factors whose splicing might be influenced by *SRSF3*. Specifically, we analysed: (i) the Song *et al.* (2019) dataset to define genes whose splicing is altered by *SRSF3* knockout; (ii) ENCORI, Encyclopedia of RNA Interactomes (Ghandi *et al.*, 2019), to identify mRNAs that physically interact with SRSF3; and (iii) GeneHancer database (Fishilevich *et al.*, 2017), to predict transcription factors capable of regulating *PDGFRB* expression (Fig. 8A). Results from these analyses revealed five genes (*TFDP1*, *CUX1*, *PRDM10*, *TEAD4* and *TP73*) that fulfil the three criteria and could thus represent a putative functional nexus between SRSF3 and PDGF-PDGFRB pathway (Fig. 8A). Indeed, analysis of PSI (Percent Spliced-in Index) of these five genes in the Song *et al.* (2019) dataset showed that *SRSF3* knockout decreased the splicing events of *TFDP1*,

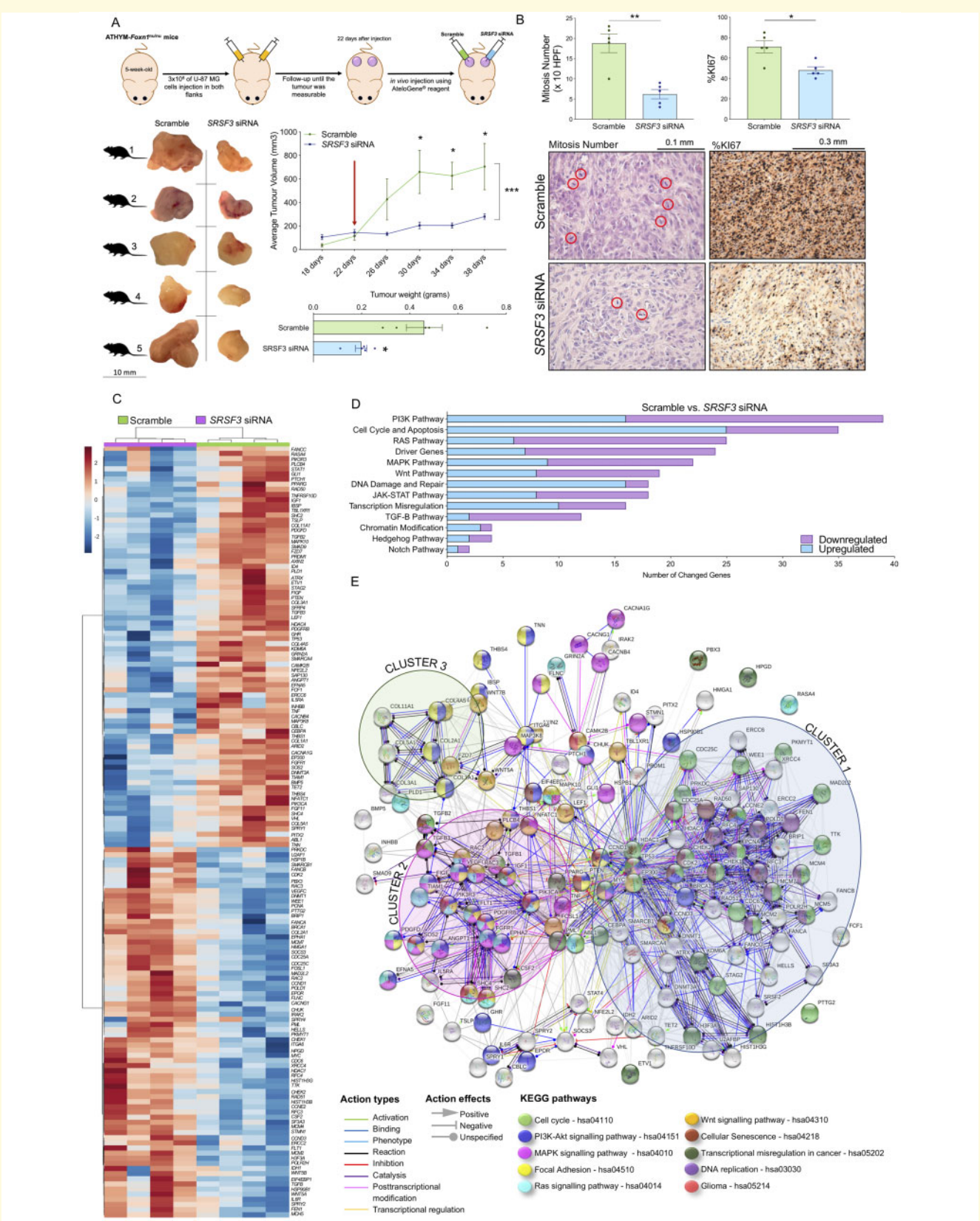

Figure 6 *SRSF3* silencing prevents the progression of glioblastomas and alters multiple key cancer related-pathways *in vivo* (U-87 MG-induced xenografts). (**A**) Diagram showing the geneneration of xenograft mouse models of glioblastoma by U-87 MG inoculation. *SRSF3 in vivo* silencing was carried out in one of the flanks of each mouse (n = 5). Average tumour volume and tumour weight of subcutaneous inoculated *SRSF3* siRNA-transfected versus scramble-transfected tumours. Images of each tumour are shown. The red arrow indicates the treatment time with scramble or *SRSF3*-siRNA using AteloGene® reagent. (**B**) Mitosis number (×10 HPF) and %KI67 IHC analysis (n = 5/group)

(continued)

CUX1 and *PRDM10*, and increased the splicing events of *TEAD4* and *TP73* (Fig. 8B and Supplementary Fig. 10C). Interestingly, from these transcription factors, only *TP73* has already been experimentally shown to directly regulate *PDGFRB* expression (Hackzell *et al.*, 2002; Uramoto *et al.*, 2004; Wetterskog *et al.*, 2009). Specifically, *TP73* has seven splicing variants due to different inclusion of its C-terminal exons (Vikhreva *et al.*, 2018), wherein only five could be experimentally detected (*TP73*α, β, γ, ε, ζ) (Fig. 8B). Some of the *TP73* splicing variants appear to differentially impact oncogenesis (e.g. *TP73*α can play an oncogenic role) (Liu *et al.*, 2004), and *TP73*β/γ variants can act as tumour suppressors (Jancalek, 2014; Vikhreva *et al.*, 2018); while the function of *TP73*ε and *TP73*ζ is still unknown. The ability of SRSF3 to influence *TP73* splicing in a GBM context is further substantiated by the altered PSI of *TP73* found in our own experimental data on *SRSF3*-silenced GBM cell lines [i.e. an increased of the MXE (Mutually eXclusive Exon) splicing event in U-87 MG and U-118 MG; Fig. 8C]. In support of a link between the modulation of the expression of *SRSF3*, changes at the level of *TP73* splicing and PDGF-PDGFRB pathway, an inverse correlation was found between MXE event PSI value of *TP73* and *PDGFRB* expression in *SRSF3*-silenced glioblastoma cells (U-87 MG and U-118 MG; Fig. 8D). Moreover, a detailed analysis of the *TP73* MXE event revealed that *SRSF3* silencing in GBM cells distinctly altered the ratio of individual splicing variants with respect to the total amount of splicing variants detected (Fig. 8E). Specifically, while *SRSF3* silencing decreased *TP73*α/*TP73* total ratio, it increased the *TP73*β-γ-ε/*TP73* total ratios (Fig. 8E).

Discussion

Glioblastoma is one of the most lethal human cancers, with late diagnosis and poor prognosis despite years of research, leading to a survival rate of 12–16 months from diagnosis (Singh and Eyras, 2017; Ostrom *et al.*, 2018). As patients are often diagnosed at advanced stages, when cure is no longer possible, their quality of life is poor and worsens rapidly, while healthcare costs concomitantly increase. Indeed, despite extensive effort made in recent years to develop therapeutic approaches for tackling this pathology (Zanders *et al.*, 2019), the current therapeutic strategies are not efficient at reducing tumour volume/growth or augmenting survival rate. This is likely due, in part, to the resistance acquired by tumours, particularly by stem cells progenitors, to current drugs (Noch *et al.*, 2018). Thus, identification of new molecular diagnostic, prognostic and therapeutic tools to refine their detection, define tumour behaviour (from tumorigenesis and progression to metastasis mechanisms) and develop new treatments is crucial to combat this devastating pathology.

The splicing process is a highly coordinated mechanism, regulated and carried out by the spliceosome, that relies on a combination of multiple spliceosome components and splicing factors, intronic and exonic sequence elements, and temporal and spatial signalling pathways to adequately control gene expression, while increasing its complex versatility (Chen and Manley, 2009; Pelechano *et al.*, 2013). Remarkably, increasing evidence over the last two decades has documented that the spliceosome and associated proteins are often altered in disease states, including metabolic diseases (Gahete *et al.*, 2018; Del Rio-Moreno *et al.*, 2019) and cancer (Dvinge *et al.*, 2016; Jia *et al.*, 2019; Jimenez-Vacas *et al.*, 2019*b*, 2020), which augments pathobiological versatility through the generation of distinct/novel alternative splicing variants (Kozlovski *et al.*, 2017; Singh and Eyras, 2017). Actually, every hallmark of cancer (Stratton *et al.*, 2009) can be associated with several examples of proto-oncogenes, tumour-suppressor genes, or other genes whose splicing is altered to produce isoforms that contribute to the transformation process (Sveen *et al.*, 2016). In fact, recent genomic characterization of different cancers has revealed recurrent copy number changes affecting genes encoding spliceosome components and splicing factors that contribute to cancer-relevant phenotype (Dvinge *et al.*, 2016). Here, we demonstrate for the first time a drastic dysregulation of the expression profile of the splicing machinery in a well-characterized cohort of HGAs/glioblastomas, where a representative set of spliceosome components and splicing factors was markedly altered (77% and 79%, respectively). Moreover, bioinformatics analyses defined an expression-based molecular fingerprint of these spliceosome components and splicing factors able to perfectly discriminate between HGAs/glioblastomas versus control tissues from both human and mouse, which further reinforces our notion, suggesting that HGAs/glioblastomas have a global splicing dysregulation in different species. Further clustering and hierarchical bioinformatics analyses in two independent human sample cohorts revealed that *SRSF3*, *RBM22*, *PTBP1* and *RBM3* were the

Figure 6 Continued
determined by experienced pathologists and representative images of haematoxylin staining of *SRSF3* siRNA-transfected versus scramble-transfected tumours. (**C**) Hierarchical heat map generated with the mRNA expression levels of significantly altered genes (n = 149) measured by nCounter PanCancer in *SRSF3* siRNA-transfected versus scramble-transfected tumours (n = 4 per group). (**D**) Number of hits of significantly altered genes in cancer-related pathways or processes. (**E**) Functional association network of the significantly altered genes in *SRSF3* siRNA-transfected versus scramble-transfected tumours. These significantly altered genes were analysed using the STRING database, and they are marked according to their KEGG pathways analysis. See also Supplementary Figs 7 and 8.

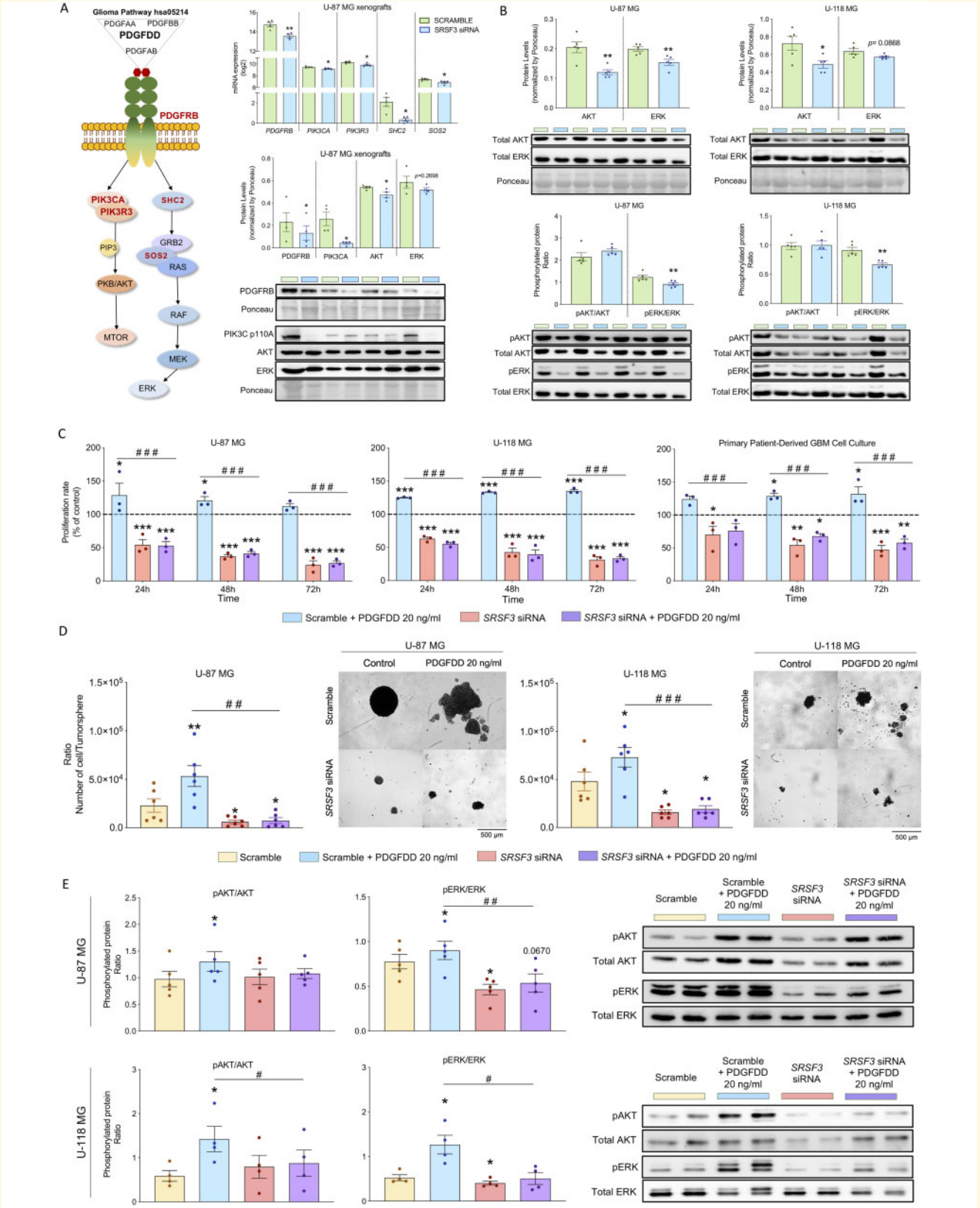

Figure 7 Inhibition of the PDGF-PDGFRB pathway as potential driver of the *SRSF3* silencing-induced anti-glioblastoma tumour actions. (**A**) Expression levels (mRNA levels measured by nCounter PanCancer and protein levels measured by western blot) of different components of the PDGFRB activated pathways (in bold) in *SRSF3* siRNA-transfected versus scramble-transfected U-87 MG-induced xenograft tumour samples (n = 4). (**B**) Phosphorylated protein ratios and total protein levels of AKT and ERK in SRSF3-silenced U-87 MG and U-118 MG cells compared to scramble-controls (n = 5) after 24 h of silencing. (**C**) Proliferation rates after treatment with PDGFDD homodimer (specific

(continued)

components of the splicing machinery with higher capacity to discriminate between human HGAs/glioblastomas and control tissues. Importantly, these results were confirmed in two independent external *in silico* cohorts of human glioblastomas (Murat/CGGA) and in different mouse glioma models analysed herein (PDGF/electroporated models). Moreover, data from the CGGA dataset also revealed that *SRSF3*, *PTBP1* and *RBM3* were significantly elevated across glioma grades (IV versus III versus II) supporting the diagnostic potential of these factors.

In this study, we evidenced an overall overexpression of SRSF3, RBM22, PTBP1 and RBM3, at both mRNA and protein level, in the different human cohorts and mouse models with gliomas analysed. Notably, silencing the expression of these splicing machinery components in glioblastoma cells induced marked reductions in aggressiveness features of glioblastomas (i.e. inhibition of proliferation, migration and VEGF secretion, and increase of apoptosis). Most notably, silencing of *SRSF3*, *RBM22*, *PTBP1* and *RBM3* strikingly decreased the number of glioblastoma stem/progenitor cells present in each tumorsphere, a relevant functional result that may help to explore how to overcome the well-known resistance of glioblastomas to current drugs (Noch *et al.*, 2018). Thus, these results demonstrate that dysregulation of the splicing machinery can play a key pathophysiological role in glioblastoma cells, and some of its components (*SRSF3*, *RBM22*, *PTBP1* and *RBM3*) could provide novel, useful tools as diagnostic biomarkers and potential therapeutic targets to tackle glioblastomas. The potential utility of *SRSF3*, *RBM22*, *PTBP1* and *RBM3* expression as prognostic biomarkers is further supported by the direct association found between their levels and relevant molecular features of aggressiveness (e.g. *MKI67*, *PCNA*, *CDK1* and *CCNB1* levels) in patients with glioblastomas but not in healthy patients, as well as between their levels and glioma grades and GBM subtypes (i.e. higher in IV versus III versus II grades, and in mesenchymal versus proneural GBM subtypes). Moreover, these observations suggested a causal link between dysregulation of these splicing machinery components and glioblastoma aggressiveness. While SRSF3, PTBP1 and RBM3, but not RBM22, have been associated with certain tumour pathologies (Guo *et al.*, 2015; Barbagallo *et al.*, 2018; Chen *et al.*, 2019*b*; Jia *et al.*, 2019; Melling *et al.*, 2019; Song *et al.*, 2019) and/or brain development (Vuong *et al.*, 2016), to the best of our knowledge, this is the first report identifying a relevant functional role of these splicing machinery components in human glioblastomas, as well as in proneural/mesenchymal-like glioma mouse models with different prognosis.

Most importantly, this study reveals that expression of *SRSF3* is directly associated with a better survival rate in HGA/glioblastoma patients, the main clinical problem in this pathology. This finding was corroborated in two external *in silico* cohorts of patients with glioblastomas (Murat and CGGA datasets), and is further supported by a recent study indicating that the knockout (KO) of *SRSF3* extended overall survival of tumour-bearing animals (Song *et al.*, 2019). In line with this, a higher *SRSF3* expression was observed in human and mouse mesenchymal GBMs (with poor survival rate) compared to proneural GBM subtypes, which reinforced the prognostic value of *SRSF3*. The mechanisms underlying the link between *SRSF3* and survival rate may relate to the direct association found between *SRSF3* silencing and tumour progression, as well as with the noteworthy disruption in one of the main pro-oncogenic signalling pathways activated in GBM cells, i.e. the PDGFRB-glioma pathway (Liu *et al.*, 2018). Specifically, we demonstrate here that *SRSF3* is an effective target in glioblastomas *in vivo*, since silencing of this splicing factor effectively blocks glioblastoma progression of already established glioblastoma tumours in a preclinical mouse model of glioblastoma. In fact, *SRSF3* silencing in glioblastoma *in vivo* markedly decreased tumour volume, tumour weight, mitosis number of glioblastoma cells and KI67 expression in all mice studied (100%), which, together with the previous *in vitro* data reported here using SRSF3-silencing glioblastoma cells, and with the extended overall survival observed in human studies, and in a recent study on KO-*SRSF3* mice (Song *et al.*, 2019), further demonstrate the clinico-pathophysiological relevance of the strong anti-tumour role of *SRSF3* silencing in glioblastomas, and its potential value as a future therapeutic target in this devastating disease. In line with our results, previous studies have also indicated that the altered expression of specific components of the splicing machinery is tightly associated with aggressive disease and poor overall survival of patients with pancreatic cancer (Qiao *et al.*, 2019) and in colorectal cancer (Sveen *et al.*, 2011).

To determine the signalling mechanisms underlying the anti-tumour role of *SRSF3* in glioblastomas, we explored an ample range of cancer-related signalling pathways in response to *SRSF3* silencing *in vivo* and *in vitro*. Our data revealed, for the first time, a striking alteration in the PI3K pathway in different *SRSF3*-silenced glioblastoma cell

Figure 7 Continued
PDGFRB ligand) on scramble-transfected versus *SRSF3*-silenced U-87 MG, U-118 MG cells and primary patient-derived glioblastoma cells (n = 3). (**D**) Number of cells per tumoursphere and representative images of formation of tumorspheres after treatment with PDGFDD homodimer (specific PDGFRB ligand) on scramble-transfected and *SRSF3*-silenced U-87 MG and U-118 MG cells (n = 6). (**E**) Phosphorylated ratio of AKT/ERK after treatment with PDGFDD homodimer (specific PDGFRB ligand) on scramble-transfected U-87 MG cells versus *SRSF3*-silenced U-87 MG (n = 5) and U-118 MG cells (n = 4). Data represent means ± SEM. *P, 0.05; **P, 0.01; ***P, 0.001, significantly different from control conditions. #P, 0.05; ##P, 0.01; ###P, 0.001, significantly different from Scramble+PDGFDD condition. See also Supplementary Fig. 9.

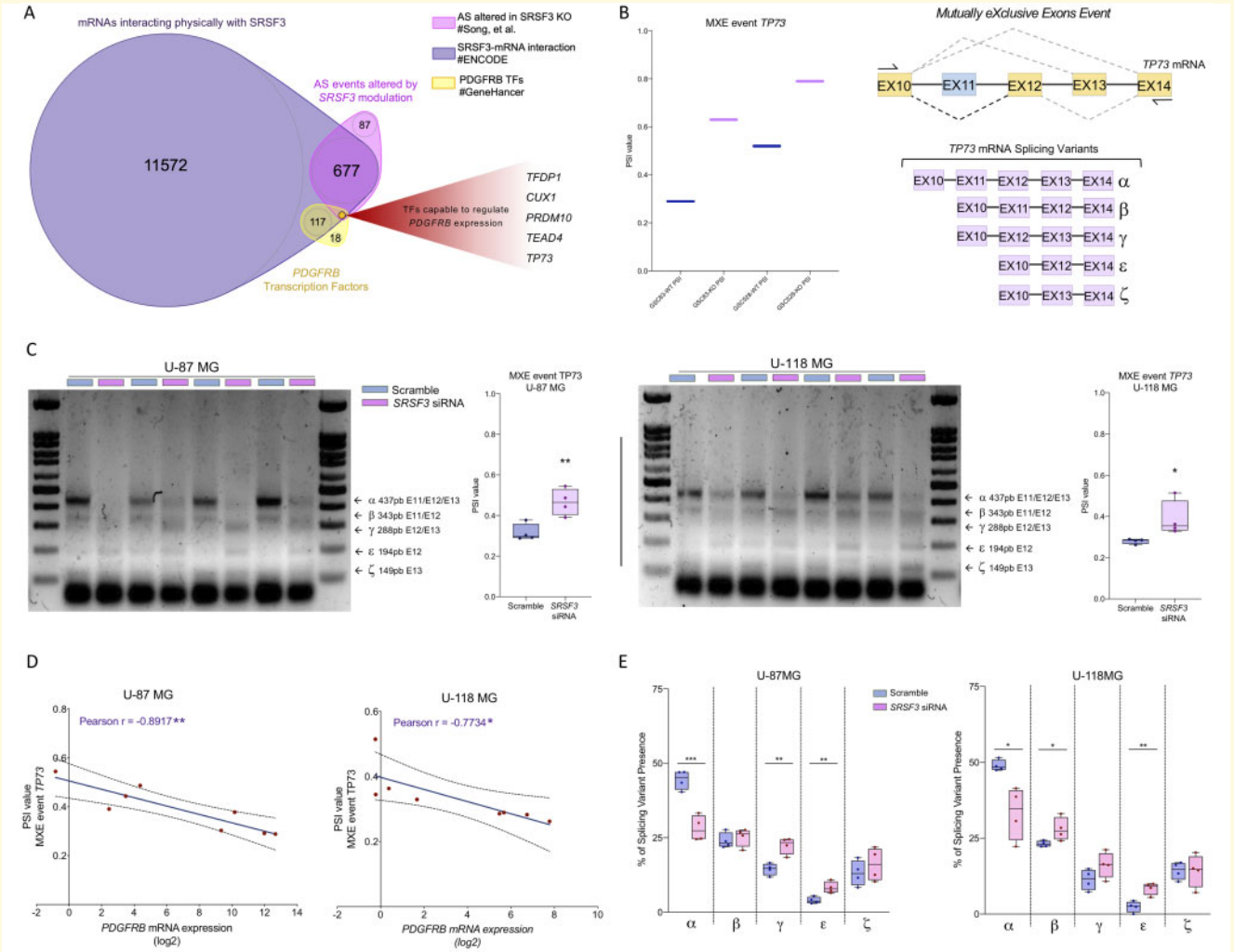

Figure 8 Changes in the expression profile of *TP73* splicing variants as potential functional link between SRSF3 and PDGF-PDGFRB pathway. (**A**) Venn diagram of three levels of information derived from different sources: Song *et al.* (2019) dataset, ENCORI (Ghandi *et al.*, 2019) and GeneHancer database (Fishilevich *et al.*, 2017). (**B**) PSI (Percent Spliced-in Index) of *TP73* from Song *et al.* (2019) dataset and diagram showing *TP73* splicing variants detected and produced by a C-terminal MXE event. (**C**) PSI of *TP73* in *SRSF3* siRNA-transfected versus scramble-transfected U-87 MG and U-118 MG cells ($n = 4$). (**D**) Correlation of *PDGFRB* mRNA expression with PSI of *TP73* in the same set of samples ($n = 4$). (**E**) Percentage of each splicing variant of *TP73* identified in *SRSF3* siRNA-transfected versus scramble-transfected U-87 MG and U-118 MG cells ($n = 4$). AS = alternative splicing. TFs = transcription factors.

models. This pathway has been reported to be closely associated with progression of glioblastomas and used as a target for the development of novel drugs (Massacesi *et al.*, 2016; Mecca *et al.*, 2018), as its inhibition or alteration causes anti-proliferative/invasive effects, and apoptosis (Mete *et al.*, 2019; Xu *et al.*, 2019). However, we found that the PDGFRB pathway, which is involved in widely known groups of glioma-related PI3K pathways (currently being used as therapeutic target) (Batchelor *et al.*, 2017), was the most relevant pathway altered in *SRSF3*-silenced cells, since a clear alteration in several genes involved in this pathway (i.e. *PDGFRB*, *SOS2*, *SHC2*, *PIK3CR3* and *PIK3CA*; all glioma pathway components) was observed. Moreover, a protein downregulation of upstream (i.e. PDGFRB and PIK3 catalytic α-subunit) and downstream (i.e. AKT) components of the glioma pathway representing classical end points for cell survival, growth and proliferation (Brennan *et al.*, 2013), was also found in *SRSF3*-silenced xenografted glioblastoma cells. Most importantly, *SRSF3* silencing blocked the stimulatory effects on AKT and ERK pathways induced by PDGFDD treatment, and completely blocked key pro-oncogenic parameters (i.e. proliferation and/or number of glioblastoma stem/progenitor cells) induced in response to PDGFDD in different glioblastoma cell models (U-87/U-118 cell lines and primary GBM cells). Therefore, these data provide original, compelling evidence that *SRSF3* is functionally linked to these well-known pathophysiologically relevant pro-oncogenic pathways in gliomas (PDGFRB and PI3K),

which further supports the potential clinico-pathophysiological importance of the strong anti-tumour role of *SRSF3* silencing in glioblastomas *in vivo* and *in vitro*.

However, SRSF3 does not appear to control PDGFRB activity by directly modulating its splicing, in that no apparent changes in *PDGFRB* splicing variants were found in *SRSF3*-silenced (this report) or in *SRSF3*-knockout (Song *et al.*, 2019) GBM cells. In contrast, SRSF3 could control the PDGFRB pathway indirectly, by modulating the alternative splicing of five potential regulators of *PDGFRB* expression such as *TFDP1*, *CUX1*, *PRDM10*, *TEAD4* and *TP73*. Previously, altered *TFDP1*, *CUX1* and *PRDM10* splicing has been reported to generate variants that act as super enhancers of several oncogenes and cell cycle checkpoint genes (Rong Zeng *et al.*, 2000; Sansregret and Nepveu, 2008; Cadieux *et al.*, 2009; Park and Kim, 2010; Hulea and Nepveu, 2012; Ramdzan and Nepveu, 2014; Lu *et al.*, 2016; Kaur *et al.*, 2018; Zhang *et al.*, 2018; Chen *et al.*, 2019*a*; Zhou *et al.*, 2020), while altered *TEAD4* splicing events could result in *VEGF* inhibition (Appukuttan *et al.*, 2012; Qi *et al.*, 2016; Xu *et al.*, 2018). Most interestingly, some splicing variants of *TP73* (the only factor reported as a *PDGFRB* regulator from the five identified) can distinctly act as tumour suppressors, arresting the cell cycle and inducing apoptosis (Liu *et al.*, 2004; Jancalek, 2014; Vikhreva *et al.*, 2018). In this scenario, it is reasonable to posit that alterations in the alternative splicing of specific transcription factors (particularly *TP73*) induced by changes in *SRSF3* expression may serve as the conduit linking SRSF3 to the PDGF-PDGFRB pathway, and thus the development/aggressiveness in glioblastoma. In support of this notion, our results indicate that *SRSF3* silencing can increase the proportion of splicing variants such as *TP73*β and *TP73*γ, which have been linked to tumour suppressor roles (Liu *et al.*, 2004) while decreasing that of the *TP73*α variant, which may play an oncogenic role (Jancalek, 2014; Vikhreva *et al.*, 2018) in glioblastoma cells. Thus, modulation of *TP73* MXE splicing event may serve as a putative mechanism linking SRSF3 and *PDGFRB* expression.

Taken together, our results unveiled new conceptual and functional avenues in glioblastomas, with potential therapeutic implications, by demonstrating for the first time a drastic dysregulation of the splicing machinery (spliceosome core and splicing factors; especially *SRSF3/RBM22/PTPB1/RBM3*) in HGAs/glioblastomas of different species. This is likely clinically relevant, because the dysregulation directly associates with development and aggressive features of glioblastomas. Moreover, we unveil a role of *SRSF3* in crucial pathophysiological processes of glioblastomas, such as cell proliferation, migration, apoptosis, VEGF secretion and tumoursphere formation, which would underlie the relevant direct association of lower *SRSF3* levels with reduced tumour progression and enhanced survival rate, observed herein in different glioblastoma human cohorts and animal models. These actions are likely mediated through the modulation of key signalling pathways (PDGFRB and PI3K) and may involve the distinct alteration of alternative splicing events of specific transcription factors controlling PDGFRB expression. Therefore, our study provides solid, convincing evidence demonstrating that *SRSF3* has a functional role in the pathophysiology of glioblastomas, and invites suggestion that the development and use of SRSF3-targeting drugs could become a promising option to treat patients with this devastating pathology, offering a clinically relevant opportunity that should be tested for use in humans.

Acknowledgement

Special thanks to GraphicalAbstractDesign.com for assistance with graph and image design.

Funding

This work was funded by the Junta de Andalucía (CTS-1406, BIO-0139), the Spanish Ministry of Science, Innovation and Universities (FPU16/05059, FPU14/04290, PID2019-105564RB-I00), Instituto de Salud Carlos III, co-funded by European Union (ERDF/ESF, 'Investing in your future': PI16/00264, PI17/02287], Spanish Ministry of Economy and Competitiveness Projects (BFU2016-80360-R, TIN2017-83445-P) and CIBERobn. M.A.B. is funded by the Spanish Ministry of Economy and Competitiveness Projects (SAF2013-45111-R and SAF2015-72455-EXP), the Comunidad de Madrid Project (S2017/BMD-3770), the World Cancer Research (WCR) Project (16-1177), and the Fundación Botín (Spain). CIBER is an initiative of Instituto de Salud Carlos III, Spanish Ministry of Health, Social Services and Equality, Spain. J.J.B. is funded by the Samuel Oschin Comprehensive Cancer Institute (SOCCI), NIH grants (R33CA236687, and R03NS101529), American Cancer Society grant (RSG-16-217-01-TBG), and SOCCI Jack Mishkin Discovery, Prevention & Genetics, and Cancer Biology Awards.

Competing interests

The authors report no competing interests.

Supplementary material

Supplementary material is available at *Brain* online.

References

Appukuttan B, et al. The related transcriptional enhancer factor-1 isoform, TEAD4(216), can repress vascular endothelial growth factor expression in mammalian cells. PLoS One 2012; 7: e31260.

Barbagallo D, .et al CircSMARCA5 inhibits migration of glioblastoma multiforme cells by regulating a molecular axis involving splicing factors SRSF1/SRSF3/PTB. Int J Mol Sci 2018; 19: 480.

Batchelor TT, et al. Feasibility, phase I, and phase II studies of tandutinib, an oral platelet-derived growth factor receptor-beta tyrosine kinase inhibitor, in patients with recurrent glioblastoma. Neuro Oncol 2017; 19: 567–75.
Bejarano L, et al. Inhibition of TRF1 telomere protein impairs tumor initiation and progression in glioblastoma mouse models and patient-derived xenografts. Cancer Cell 2017; 32: 590–607.e4.
Bowman RL, et al. GlioVis data portal for visualization and analysis of brain tumor expression datasets. Neuro Oncol 2017; 19: 139–41.,
Brennan CW, et al. The somatic genomic landscape of glioblastoma. Cell 2013; 155: 462–77.
Breunig JJ, et al. Ets factors regulate neural stem cell depletion and gliogenesis in Ras pathway glioma. Cell Rep 2016; 17: 3407.
Cadieux C, et al. Mouse mammary tumor virus p75 and p110 CUX1 transgenic mice develop mammary tumors of various histologic types. Cancer Res 2009; 69: 7188–97.
Chen M, Manley JL. Mechanisms of alternative splicing regulation: insights from molecular and genomics approaches. Nat Rev Mol Cell Biol 2009; 10: 741–54.
Chen N, et al. Transcriptional regulation of Bcl-2 gene by the PR/SET domain family member PRDM10. PeerJ 2019a; 7: e6941.
Chen P, et al. RBM3 upregulates ARPC2 by binding the 3'UTR and contributes to breast cancer progression. Int J Oncol 2019b; 54: 1387–97.
Cordoba-Chacon J, et al. Truncated somatostatin receptors as new players in somatostatin-cortistatin pathophysiology. Ann N Y Acad Sci 2011; 1220: 6–15.
Del Rio-Moreno M, et al. Dysregulation of the splicing machinery is associated to the development of nonalcoholic fatty liver disease. J Clin Endocrinol Metab 2019; 104: 3389–402.
Duran-Prado M, et al. Identification and characterization of two novel truncated but functional isoforms of the somatostatin receptor subtype 5 differentially present in pituitary tumors. J Clin Endocrinol Metab 2009; 94: 2634–43.
Dvinge H, et al. RNA splicing factors as oncoproteins and tum suppressors. Nat Rev Cancer 2016; 16: 413–30.
Edwards NJ, et al. The CPTAC data portal: a resource for cancer proteomics research. J Proteome Res 2015; 14: 2707–13.,
Feero WG, Guttmacher AE, Collins FS. Genomic medicine–an updated primer. N Engl J Med 2010; 362: 2001–11.
Fishilevich S, et al. GeneHancer: genome-wide integration of enhancers and target genes in GeneCards. Database (Oxford) 2017; 2017: bax028.
Gahete MD, et al. Changes in splicing machinery components influence, precede, and early predict the development of type 2 diabetes: from the CORDIOPREV study. EBioMedicine 2018; 37: 356–36.
Ghandi M, et al. Next-generation characterization of the Cancer Cell Line Encyclopedia. Nature 2019; 569: 503–8.
Guo J, Jia J, Jia R. PTBP1 and PTBP2 impaired autoregulation of SRSF3 in cancer cells. Sci Rep 2015; 5: 14548.
Hackzell A, et al. p73 independent of c-Myc represses transcription of platelet-derived growth factor beta-receptor through interaction with NF-Y. J Biol Chem 2002; 277: 39769–76.
Hormaechea-Agulla D, et al. Ghrelin O-acyltransferase (GOAT) enzyme is overexpressed in prostate cancer, and its levels are associated with patient's metabolic status: potential value as a non-invasive biomarker. Cancer Lett 2016; 383: 125–34.
Hormaechea-Agulla D, et al. The oncogenic role of the In1-ghrelin splicing variant in prostate cancer aggressiveness. Mol Cancer 2017a; 16: 146.
Hormaechea-Agulla D, et al. The oncogenic role of the spliced somatostatin receptor sst5TMD4 variant in prostate cancer. FASEB J 2017b; 31: 4682–96.
Hulea L, Nepveu A. CUX1 transcription factors: from biochemical activities and cell-based assays to mouse models and human diseases. Gene 2012; 497: 18–26.
Jancalek R. The role of the TP73 gene and its transcripts in neuro-oncology. Br J Neurosurg 2014; 28: 598–605.
Jia R, et al. Oncogenic splicing factor SRSF3 regulates ILF3 alternative splicing to promote cancer cell proliferation and transformation. RNA 2019; 25: 630–44.
Jimenez-Vacas JM, et al. Spliceosome component SF3B1 as novel prognostic biomarker and therapeutic target for prostate cancer. Transl Res 2019a; 212: 89–103.
Jimenez-Vacas JM, et al. Spliceosome component SF3B1 as novel prognostic biomarker and therapeutic target for prostate cancer. Transl Res 2019b; 212: 89–103.
Jimenez-Vacas JM, et al. Dysregulation of the splicing machinery is directly associated to aggressiveness of prostate cancer. EBioMedicine 2020; 51: 102547.
Jiménez-Vacas JM, et al. Clinical utility of Ghrelin-O-Acyltransferase (GOAT) enzyme as a diagnostic tool and potential therapeutic target in prostate cancer. J Clin Med 2019; 8: 2056.
Jurica MS, Moore MJ. Pre-mRNA splicing: awash in a sea of proteins. Mol Cell 2003; 12: 5–14.
Kaur S, et al. CUX1 stimulates APE1 enzymatic activity and increases the resistance of glioblastoma cells to the mono-alkylating agent temozolomide. Neuro Oncol 2018; 20: 484–93.
Kozlovski I, et al. The role of RNA alternative splicing in regulating cancer metabolism. Hum Genet 2017; 136: 1113–27.
Liu G, et al. DeltaNp73beta is active in transactivation and growth suppression. Mol Cell Biol 2004; 24: 487–501.
Liu T, et al. PDGF-mediated mesenchymal transformation renders endothelial resistance to anti-VEGF treatment in glioblastoma. Nat Commun 2018; 9: 3439.
Louis DN, et al. The 2016 World Health Organization classification of tumors of the central nervous system: a summary. Acta Neuropathol 2016; 131: 803–20.
Lu X, et al. Dysregulation of TFDP1 and of the cell cycle pathway in high-grade glioblastoma multiforme: a bioinformatic analysis. Genet Mol Res 2016; 15: gmr7646.
Luque RM, et al. A cellular and molecular basis for the selective desmopressin-induced ACTH release in Cushing disease patients: key role of AVPR1b receptor and potential therapeutic implications. J Clin Endocrinol Metab 2013; 98: 4160–9.
Luque RM, et al. Truncated somatostatin receptor variant sst5TMD4 confers aggressive features (proliferation, invasion and reduced octreotide response) to somatotropinomas. Cancer Lett 2015; 359: 299–306.
Massacesi C, et al. PI3K inhibitors as new cancer therapeutics: implications for clinical trial design. Onco Targets Ther 2016; 9: 203–10.
Matera AG, Wang Z. A day in the life of the spliceosome. Nat Rev Mol Cell Biol 2014; 15: 108–21.
Mecca C, et al. Targeting mTOR in glioblastoma: rationale and preclinical/clinical evidence. Dis Markers 2018; 2018: 9230479.
Melling N, et al. Prevalence and clinical significance of RBM3 immunostaining in non-small cell lung cancers. J Cancer Res Clin Oncol 2019; 145: 873–9.
Mete M, et al. Punicic acid inhibits glioblastoma migration and proliferation via the PI3K/AKT1/mTOR signaling pathway. Anticancer Agents Med Chem 2019; 19: 1120–31.
Murat A, et al. Stem cell-related "self-renewal" signature and high epidermal growth factor receptor expression associated with resistance to concomitant chemoradiotherapy in glioblastoma. J Clinc Oncol 2008; 26: 3015–24.
Noch EK, Ramakrishna R, Magge R. Challenges in the treatment of glioblastoma: multisystem mechanisms of therapeutic resistance. World Neurosurg 2018; 116: 505–17.
Ostrom QT, et al. CBTRUS statistical report: primary brain and other central nervous system tumors diagnosed in the United States in 2011-2015. Neuro Oncol 2018; 20: iv1–iv86.
Ozawa T, et al. Most human non-GCIMP glioblastoma subtypes evolve from a common proneural-like precursor glioma. Cancer Cell 2014; 26: 288–300.

Ozdemir-Kaynak E, Qutub AA, Yesil-Celiktas O. Advances in glioblastoma multiforme treatment: new models for nanoparticle therapy. Front Physiol 2018; 9: 170.
Park JA, Kim KC. Expression patterns of PRDM10 during mouse embryonic development. BMB Rep 2010; 43: 29–33.
Pelechano V, Wei W, Steinmetz LM. Extensive transcriptional heterogeneity revealed by isoform profiling. Nature 2013; 497: 127–31.
Qi Y, et al. A splicing isoform of TEAD4 attenuates the Hippo-YAP signalling to inhibit tum proliferation. Nat Commun 2016; 7: ncomms11840.
Qiao L, et al. Identification of upregulated HNRNPs associated with poor prognosis in pancreatic cancer. Biomed Res Int 2019; 2019: 5134050.
Ramdzan ZM, Nepveu A. CUX1, a haploinsufficient tum suppressor gene overexpressed in advanced cancers. Nat Rev Cancer 2014; 14: 673–82.
Rong Zeng W, et al. Exon/intron structure and alternative transcripts of the CUTL1 gene. Gene 2000; 241: 75–85.
Sansregret L, Nepveu A. The multiple roles of CUX1: insights from mouse models and cell-based assays. Gene 2008; 412: 84–94.
Sarmento-Cabral A, et al. Metformin reduces prostate tumor growth, in a diet-dependent manner, by modulating multiple signaling pathways. Mol Cancer Res 2017; 15: 862–74.
Schneider CA, Rasband WS, Eliceiri KW. NIH Image to ImageJ: 25 years of image analysis. Nat Methods 2012; 9: 671–5.
Singh B, Eyras E. The role of alternative splicing in cancer. Transcription 2017; 8: 91–8.
Song X, et al. SRSF3-regulated RNA alternative splicing promotes glioblastoma tumorigenicity by affecting multiple cellular processes. Cancer Res 2019; 79: 5288–301.
Stratton MR, Campbell PJ, Futreal PA. The cancer genome. Nature 2009; 458: 719–24.
Stringer BW, et al. A reference collection of patient-derived cell line and xenograft models of proneural, classical and mesenchymal glioblastoma. Sci Rep 2019; 9: 4902.
Sveen A, et al. Transcriptome instability in colorectal cancer identified by exon microarray analyses: associations with splicing factor expression levels and patient survival. Genome Med 2011; 3: 32.
Sveen A, et al. Aberrant RNA splicing in cancer; expression changes and driver mutations of splicing factor genes. Oncogene 2016; 35: 2413–27.
Uphoff CC, Drexler HG. Detection of mycoplasma contaminations. Methods Mol Biol 2013; 946: 1–13.
Uramoto H, et al. p73 competes with co-activators and recruits histone deacetylase to NF-Y in the repression of PDGF beta-receptor. J Cell Sci 2004; 117: 5323–31.
Vazquez-Borrego MC, et al. A somatostatin receptor subtype-3 (SST3) peptide agonist shows antitumor effects in experimental models of Nonfunctioning Pituitary Tumors. Clin Cancer Res 2019; 26: 957–69.
Vikhreva P, Melino G, Amelio I. p73 Alternative splicing: exploring a biological role for the c-terminal isoforms. J Mol Biol 2018; 430: 1829–38.
Vuong JK, et al. PTBP1 and PTBP2 serve both specific and redundant functions in neuronal Pre-mRNA splicing. Cell Rep 2016; 17: 2766–75.
Wetterskog D, et al. Dysregulation of platelet-derived growth factor beta-receptor expression by DeltaNp73 in neuroblastoma. Mol Cancer Res 2009; 7: 2031–9.
Xu A, et al. Overexpression of TEAD4 correlates with poor prognosis of glioma and promotes cell invasion. Int J Clin Exp Pathol 2018; 11: 4827–35.
Xu PF, et al. PI3Kbeta inhibitor AZD6482 exerts antiproliferative activity and induces apoptosis in human glioblastoma cells. Oncol Rep 2019; 41: 125–32.
Yan C, Wan R, Shi Y. Molecular mechanisms of pre-mRNA splicing through structural biology of the spliceosome. Cold Spring Harb Perspect Biol 2019; 11: a032409.
Zanders ED, Svensson F, Bailey DS. Therapy for glioblastoma: is it working?. Drug Discov Today 2019; 24: 1193–201.
Zhang L, et al. Screening and function analysis of hub genes and pathways in hepatocellular carcinoma via bioinformatics approaches. Cancer Biomark 2018; 22: 511–21.
Zhou J, et al. Identification of chemoresistance-related mRNAs based on gemcitabine-resistant pancreatic cancer cell lines. Cancer Med 2020; 9: 1115–30.